

# Heavy quarkonium dissociation cross sections in relativistic heavy-ion collisions

Cheuk-Yin Wong,<sup>1</sup> E. S. Swanson,<sup>2,3</sup> and T. Barnes<sup>1,4</sup>

<sup>1</sup>*Physics Division, Oak Ridge National Laboratory, Oak Ridge, Tennessee 37831*

<sup>2</sup>*Department of Physics and Astronomy, University of Pittsburgh, Pittsburgh, Pennsylvania 15260*

<sup>3</sup>*Jefferson Lab, Newport News, Virginia 23606*

<sup>4</sup>*Department of Physics, University of Tennessee, Knoxville, Tennessee 37996*

(Received 29 June 2001; published 3 December 2001)

Many of the hadron-hadron cross sections required for the study of the dynamics of matter produced in relativistic heavy-ion collisions can be calculated using the quark-interchange model. Here we evaluate the low-energy dissociation cross sections of  $J/\psi$ ,  $\psi'$ ,  $\chi$ ,  $\Upsilon$ , and  $\Upsilon'$  in collision with  $\pi$ ,  $\rho$ , and  $K$ . These are important for the interpretation of heavy-quarkonium suppression as a signature for the quark gluon plasma, as such comover dissociation processes also contribute to heavy-quarkonium suppression, and must be understood and incorporated in simulations of heavy-ion collisions before QGP formation can be established through this signature.

DOI: 10.1103/PhysRevC.65.014903

PACS number(s): 25.75.-q, 13.75.Gx, 12.39.-x, 25.80.Ls

## I. INTRODUCTION

The first collisions of heavy-ion beams at the Relativistic Heavy-Ion Collider (RHIC) at Brookhaven National Laboratory heralded a new era in the study of matter in the extreme conditions of very high-temperatures and energy densities. The ultimate goal of this research is the production of a quark-gluon plasma (QGP), which is an unusual phase of strongly interacting matter that purportedly existed shortly after the big bang [1,2].

The search for the quark-gluon plasma relies on the unusual properties of the plasma for its detection. However, many conventional hadrons are also produced during heavy-ion collisions. Whatever signal is chosen for the identification of the quark-gluon plasma, contributions to that signal from conventional hadronic processes must be identified as backgrounds and removed from the data.

Although there are recent, tantalizing hints of possible quark-gluon plasma production in heavy-ion collisions at CERN [3,4], conclusive evidence is still lacking due to uncertain backgrounds from conventional hadronic sources. Investigations of the various “hadronic background processes” are urgently needed if we are to develop a satisfactory understanding of the various signals proposed as signatures of a quark-gluon plasma. In this paper we consider one type of hadronic background processes that can contribute to heavy-quarkonium suppression, which is frequently cited as a QGP signature.

Matsui and Satz [5] originally suggested the use of suppressed  $J/\psi$  production as a signature for the formation of a quark-gluon plasma in high-energy heavy-ion collisions. The recent experimental observation of anomalous  $J/\psi$  suppression in Pb+Pb collisions by the NA50 Collaboration [6,7] has been considered by many authors [8–17]. However, there is considerable uncertainty in these studies, due to the lack of reliable experimental information on  $J/\psi$  and  $\chi_J$  dissociation cross sections in low-energy collisions with light hadrons. Because heavy quarkonia decay strongly, many of the dissociation cross sections cannot be measured directly in hadron scattering experiments; the cross sections are instead

typically estimated using theoretical models. Evaluation of these cross sections is of particular interest for clarifying the physics of the  $J/\psi$  anomalies observed in Pb-Pb collisions and may be of considerable importance in future  $J/\psi$  studies using the RHIC and LHC colliders.

The dissociation of the  $J/\psi$  by hadrons has been considered previously in several theoretical studies, but the predicted cross sections show great variation at low energies, largely due to different assumptions regarding the dominant scattering mechanism [18–28].

Kharzeev and collaborators [18,19] employed the parton model and perturbative QCD “short-distance” approach of Bhanot and Peskin [29,30] and found remarkably small low-energy cross sections for collisions of  $J/\psi$  with light hadrons. For example, their  $J/\psi+N$  cross section at  $\sqrt{s}=5$  GeV is only about  $0.25 \mu\text{b}$  [18]. A finite-mass correction increases this cross section by about a factor of 2 [19]. However, in high-energy heavy-ion reactions the collisions between the produced  $\pi$  and  $\rho$  with  $J/\psi$  and  $\psi'$  occur at low energies (typically from a few hundred MeV to about 1 GeV relative kinetic energies). The applicability of the parton model and perturbative QCD (PQCD) for reactions in this low-energy region is certainly open to question.

Matinyan and Müller [24], Haglin [25], Lin and Ko [26], and Oh, Song, and Lee [27] recently reported results for these dissociation cross sections in meson exchange models. These references all use effective meson Lagrangians, but differ in the interaction terms included in the Lagrangian. Matinyan and Müller included only  $t$ -channel  $D$ -meson exchange and found that the dissociation cross sections of  $J/\psi$  by  $\pi$  and  $\rho$  are rather small; both are  $\approx 0.2\text{--}0.3$  mb at  $\sqrt{s}=4$  GeV. Including form factors (arbitrarily chosen to be Gaussians with a width set to 1.5 GeV) would reduce these cross sections by an order of magnitude. Haglin obtained a very different result, with much larger cross sections, by treating the  $D$  and  $D^*$  mesons as non-Abelian gauge bosons in a minimally coupled Yang-Mills meson Lagrangian. Form factors were also introduced in these calculations [25–27]. The resulting mb-scale cross sections are very sensitive to

the choice of form factors. Charmonium dissociation by nucleons has also been considered recently using a similar effective Lagrangian formulation [28]. Of course, the use of a Yang-Mills Lagrangian for charmed mesons has no *a priori* justification, so this crucial initial assumption made in these references requires independent confirmation. The assumption of the *t*-channel exchange of a heavy meson such as a *D* or *D\** between a hadron and a *J/ψ* is also difficult to justify physically, because the range of these exchanges ( $1/M \approx 0.1$  fm) is much smaller than the physical extent of the initial hadron and the *J/ψ*.

Another method which has been used to study charmonium dissociation is to determine these amplitudes using quark model wave functions for the external hadrons and the well-established interquark forces as the scattering Hamiltonian. In the low-energy “resonance” regime we are considering, we expect that this approach will give a reasonably accurate description of the hadronic scattering amplitudes.

Martins, Blaschke, and Quack [20] previously reported dissociation cross section calculations using essentially the same approach we describe here. The short-distance interaction used by these authors in particular is quite similar to the form we employ. For the confining interaction, however, they used a simplified color-independent Gaussian potential between quark-antiquark pairs, rather than the now well-established linear  $\lambda(i) \cdot \lambda(j)$  form. They found a rather large  $\pi + J/\psi$  dissociation cross section, which reached a maximum of about 7 mb at a center-of-mass kinetic energy  $E_{KE}$  of about 0.85 GeV. Although our approach is very similar to that of Martins *et al.*, our final numerical results differ significantly, due mainly to our different treatments of the confining interaction.

In this paper we use the approach discussed above to evaluate the dissociation cross sections of *J/ψ*,  $\psi'$ ,  $\chi$ ,  $\Upsilon$ , and  $\Upsilon'$  in collision with  $\pi$ ,  $\rho$ , and *K*, and compare our results to other theoretical cross sections reported in the literature. The dissociation cross sections of  $\chi_J$  mesons are of special interest, as an estimated 1/3 of the *J/ψ* mesons produced in high-energy nucleon-nucleon collisions come from the decay of  $\chi$  states [31]. The dissociation cross sections for  $\Upsilon$  are also interesting, and they have recently been estimated to be quite small in an effective-Lagrangian meson-exchange model, due to the large thresholds for dissociation of  $\Upsilon$  by both  $\pi$  and  $\rho$  [32].

We employ the Barnes-Swanson quark-interchange model [33,34] to evaluate these dissociation cross sections in terms of wave functions and interactions at the quark level. We use the nonrelativistic quark potential model and its interquark Hamiltonian to describe the underlying quark-gluon forces. The model parameters and quark masses are determined by the meson spectrum, so there is little additional freedom in determining scattering amplitudes and cross sections. We thus implicitly incorporate the successes of the quark model in describing the meson spectrum and many static and dynamical properties of hadrons. We proceed by calculating the scattering amplitude for a given process at Born order in the interquark Hamiltonian; the good agreement of this approach with experimental scattering data on many low-energy reactions [33–36] provides strong motivation for the application

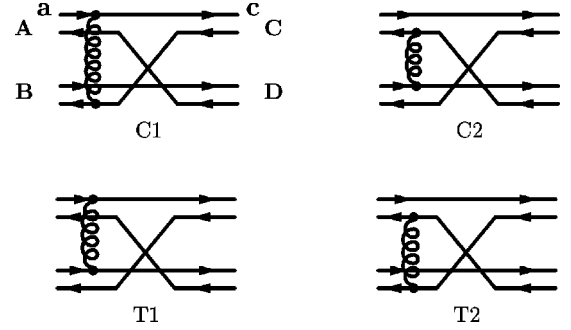


FIG. 1. “Prior” diagrams for Born-order meson-meson scattering.

of this approach to hadron reactions in relativistic heavy-ion collisions. A brief summary of the present work has been reported previously [21].

This paper is organized as follows. In Sec. II we summarize the Barnes-Swanson model of quark interchange as applied to the calculations of the dissociation cross sections. The reaction matrix can be described in terms of the “prior” or “post” diagrams, which are discussed in Sec. III. Section IV gives some details of the evaluation of the spin and spatial matrix elements for the general meson-meson scattering problem. In Sec. V the spin matrix elements are derived explicitly in terms of  $9j$  symbols. The evaluation of spatial overlap integrals for the case of all *S*-wave mesons is discussed in Sec. VI. In Sec. VII, we evaluate the corresponding overlap integrals for one *P*-wave meson. An accurate determination of these matrix elements requires correspondingly accurate bound-state wave functions; the evaluation of these wave functions is discussed in Sec. VIII. Numerical agreement between post and prior scattering amplitudes is shown explicitly in Sec. IX, and provides a very nontrivial check of the accuracy and internal consistency of our calculations. Section X presents our results for the dissociation cross section of *J/ψ* and  $\psi'$  in collision with various light mesons, and Sec. XI gives the corresponding cross sections for the dissociation of  $\Upsilon$  and  $\Upsilon'$ . Section XII present results for the dissociation of *P*-wave charmonium states, the  $\chi_J$  mesons, in collision with  $\pi$ ,  $\rho$ , and *K*. Finally, we give our conclusions in Sec. XIII.

## II. MODEL

We shall briefly summarize the model of Barnes and Swanson for constituent-interchange processes in the reaction

$$A(12) + B(34) \rightarrow C(14) + D(32), \quad (1)$$

where *A*, *B*, *C*, and *D* are  $q\bar{q}$  mesons, and 1, 3 and 2, 4 label the quark and antiquark constituents, respectively. In this meson-meson scattering problem the scattering amplitude in the “prior formalism” is the sum of the four quark-line diagrams of Fig. 1. These are evaluated as overlap integrals of quark model wave functions using the Feynman rules given in Appendix C of Ref. [33]. This method has previously been applied successfully to the closely related no-

annihilation scattering channels  $I=2 \pi\pi$  [33],  $I=3/2 K\pi$  [35],  $I=\{0,1\}$   $S$ -wave  $KN$  scattering [36], the short-range repulsive  $NN$  interaction [37], and pseudoscalar-vector scatterings [38].

The interaction  $H_{ij}(r_{ij})$  between a pair of constituents  $i$  and  $j$  is represented by the curly line in Fig. 1, and is taken to be

$$\begin{aligned} H_{ij}(r_{ij}) &= \frac{\boldsymbol{\lambda}(i)}{2} \cdot \frac{\boldsymbol{\lambda}(j)}{2} \{V_{\text{color-Coulomb}}(r_{ij}) + V_{\text{linear}}(r_{ij}) \\ &\quad + V_{\text{spin-spin}}(r_{ij}) + V_{\text{con}}\} \\ &= \frac{\boldsymbol{\lambda}(i)}{2} \cdot \frac{\boldsymbol{\lambda}(j)}{2} \\ &\quad \times \left\{ \frac{\alpha_s}{r_{ij}} - \frac{3b}{4} r_{ij} - \frac{8\pi\alpha_s}{3m_i m_j} \mathbf{s}_i \cdot \mathbf{s}_j \left( \frac{\sigma^3}{\pi^{3/2}} \right) \right. \\ &\quad \left. \times e^{-\sigma^2 r_{ij}^2} + V_{\text{con}} \right\}, \end{aligned} \quad (2)$$

where  $\alpha_s$  is the strong coupling constant,  $b$  is the string tension,  $m_i$  and  $m_j$  are the masses of the interacting constituents,  $\sigma$  is the range parameter in the hyperfine spin-spin interaction, and  $V_{\text{con}}$  is a constant. For an antiquark the generator  $\boldsymbol{\lambda}/2$  is replaced by  $-\boldsymbol{\lambda}^T/2$ .

It is convenient to introduce  $V_{ij}(r_{ij})$  to denote the quantity in curly brackets in Eq. (2) so that we can write  $H_{ij}(\mathbf{r}_{ij})$  in the form

$$H_{ij}(\mathbf{r}_{ij}) = \frac{\boldsymbol{\lambda}(i)}{2} \cdot \frac{\boldsymbol{\lambda}(j)}{2} V_{ij}(r_{ij}). \quad (3)$$

The Born-order  $T$ -matrix element  $T_{fi}$  is proportional to the matrix elements  $h_{fi}$  of this residual interaction (as defined in Ref. [33]). For each of the scattering diagrams of Fig. 1,  $h_{ij}$  and  $T_{ij}$  are given as the product of four factors,

$$h_{fi} = \frac{1}{(2\pi)^3} T_{fi} = S I_{\text{flavor}} I_{\text{color}} I_{\text{spin-space}}. \quad (4)$$

The overall sign  $S$  is a fermion-permutation phase known as the ‘‘signature’’ of the diagram, which is equal to  $(-1)^{N_x}$ , where  $N_x$  is the number of fermion line crossings. ( $S = -1$  for the diagrams in Fig. 1.) The flavor matrix element  $I_{\text{flavor}}$  is the overlap of the initial and final flavor wave functions. In all the processes considered in this paper,  $I_{\text{flavor}}$  is equal to 1 for all diagrams. The color matrix element  $I_{\text{color}}$  is  $-4/9$  for diagrams C1 and C2, and is  $+4/9$  for diagrams T1 and T2. The spatial and spin matrix element  $I_{\text{spin-space}}$  is the matrix element of  $V_{ij}$ , and can in general be written as a sum of products of a spin matrix element  $I_{\text{spin}}$  times a spatial matrix element  $I_{\text{space}}$ . The spin matrix element  $I_{\text{spin}}$  involves Clebsch-Gordon coefficients and the spins of the colliding particles and is tabulated for all cases of  $S$ -wave mesons in [33]. An explicit closed-form expression for this  $I_{\text{spin}}$  in terms of Wigner’s  $9j$  symbol will be given in Sec. V. The

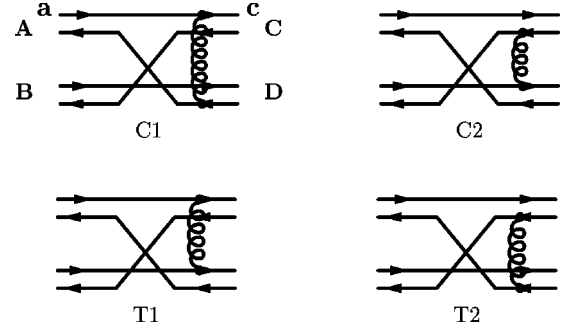


FIG. 2. ‘‘Post’’ diagrams for Born-order meson-meson scattering.

evaluation of the spatial matrix element  $I_{\text{space}}$  will be discussed in detail in Secs. VI and VII.

For the reaction  $A + B \rightarrow C + D$ , with an invariant momentum transfer  $t$ ,

$$t = (A - C)^2 = m_A^2 + m_C^2 - 2A_0 C_0 + 2\mathbf{A} \cdot \mathbf{C}, \quad (5)$$

the differential cross section is given by

$$\frac{d\sigma_{fi}}{dt} = \frac{1}{64\pi s |\mathbf{p}_A|^2} |\mathcal{M}_{fi}|^2, \quad (6)$$

where the matrix element  $\mathcal{M}_{fi}$  is related to  $T_{fi}$  by

$$\mathcal{M}_{fi} = \sqrt{(2E_A)(2E_B)(2E_C)(2E_D)} T_{fi}. \quad (7)$$

In Eqs. (6) and (7),  $\mathbf{p}_A$  and  $E_A$  are the momentum and the energy of meson  $A$  in the center-of-mass system. The total cross section for the reaction  $A + B \rightarrow C + D$  can be obtained from  $d\sigma_{fi}/dt$  by integrating over  $t$ .

### III. POST AND PRIOR DESCRIPTIONS

Before proceeding to our results, we note that a well-known ‘‘post-prior ambiguity’’ arises in the calculation of bound-state scattering amplitudes involving rearrangement collisions [39]. Since the Hamiltonian which describes the scattering process  $AB \rightarrow CD$  can be separated into an unperturbed Hamiltonian and a residual interaction in two ways,  $H = H_A^{(0)} + H_B^{(0)} + V_{AB} = H_C^{(0)} + H_D^{(0)} + V_{CD}$ , there is an ambiguity in the choice of  $V_{AB}$  or  $V_{CD}$  as the residual interaction. The first version gives the ‘‘prior’’ diagrams of Fig. 1, in which the interaction occurs before constituent interchange. The second choice is the ‘‘post’’ formalism in which the interaction occurs after constituent interchange, as in the diagrams of Fig. 2.

One may prove in the context of nonrelativistic quantum mechanics that the prior and post diagrams give the same scattering amplitude and hence the same cross section, provided that exact bound-state wave functions of the various  $\{H^{(0)}\}$  are used for the external states [39]. (This was discussed in detail and demonstrated numerically for  $\pi\pi \rightarrow \rho\rho$  scattering in Ref. [34], where its relevance to establishing Hermitian effective scattering potentials was shown.) A consistent calculation thus leads to description-identical results

for the scattering amplitude in nonrelativistic quantum mechanics. We shall confirm the prior-post equivalence numerically in our nonrelativistic calculations of the  $J/\psi$  and  $\psi'$  dissociation cross sections.

#### IV. EVALUATION OF THE MATRIX ELEMENT $I_{\text{SPIN-SPACE}}$

For the processes considered here it suffices to treat reactions of the form  $A(12) + B(34) \rightarrow C(14) + D(32)$ , in which constituents (antiquarks) 2 and 4 are interchanged, as depicted in Figs. 1 and 2. We denote the total angular momentum, the orbital angular momentum, and the spin of meson  $a$  ( $a=A, B, C$ , and  $D$ ) by  $J_a, L_a$ , and  $S_a$ , respectively, with an associated spatial wave function  $\Phi_a$  and spin wave function  $\chi_a$ .

The quantity  $I_{\text{spin-space}}$  is the matrix element of  $V_{ij}(r_{ij})$  between the initial and final meson states. The interaction

$V_{ij}(r_{ij})$  is the spin and spatial part of  $H_{ij}$  [Eqs. (2) and (3)], and consists of the sum

$$V_{ij}(r_{ij}) = \sum_i^3 v_r^{(i)} v_s^{(i)} + V_{\text{con}}, \quad (8)$$

where the superscripts  $(i)$  refer to color-Coulomb, linear, and spin-spin interactions, respectively. Specifically,  $v_s^{(1)} = v_s^{(2)} = 1$ ,  $v_s^{(3)} = s_i \cdot s_j$ , and the corresponding  $v_r^{(i)}$  can be read from Eqs. (2) and (3). For the scattering problem the sum of the amplitudes of all diagrams arising from the constant term  $V_{\text{con}}$  is zero, so we need not include  $V_{\text{con}}$  in deriving scattering amplitudes and matrix elements.

The matrix element  $I_{\text{spin-space}}$  is therefore the sum of three terms, each of which is of the form

$$\begin{aligned} \langle (\Phi_C \chi_C)_{J_{Cz}}^{J_C} (\Phi_D \chi_D)_{J_{Dz}}^{J_D} | v_r v_s | (\Phi_A \chi_A)_{J_{Az}}^{J_A} (\Phi_B \chi_B)_{J_{Bz}}^{J_B} \rangle = \sum_{JJ_z J'_z} (J_C J_{Cz} J_D J_{Dz} | J' J'_z) (J J_z | J_A J_{Az} J_B J_{Bz}) \\ \times \langle [(\Phi_C \chi_C)^{J_C} (\Phi_D \chi_D)^{J_D}]_{J_z}^{J'} | v_r v_s | [(\Phi_A \chi_A)^{J_A} (\Phi_B \chi_B)^{J_B}]_{J_z}^J \rangle. \end{aligned} \quad (9)$$

In the above equation, the coupled initial state  $[[(\Phi_A \chi_A)^{J_A} (\Phi_B \chi_B)^{J_B}]_{J_z}^J] \equiv |\Psi_{\text{in}}^{JJ_z}\rangle$  of mesons  $A(12)$  and  $B(34)$  can be written as [40]

$$\begin{aligned} |\Psi_{\text{in}}^{JJ_z}\rangle = \sum_{S,L} \langle (\chi_A \chi_B)^S (\Phi_A \Phi_B)^L J J_z | (\Phi_A \chi_A)^{J_A} (\Phi_B \chi_B)^{J_B} J J_z \rangle [(\chi_A \chi_B)^S (\Phi_A \Phi_B)^L]_{J_z}^J \\ = \sum_{SLS_z} \hat{S} \hat{L} \hat{J}_A \hat{J}_B \begin{Bmatrix} S_A & S_B & S \\ L_A & L_B & L \\ J_A & J_B & J \end{Bmatrix} (SS_z L(J_z - S_z) | J J_z) (\chi_A \chi_B)_{S_z}^S (\Phi_A \Phi_B)_{(J_z - S_z)}^L, \end{aligned} \quad (10)$$

where  $\hat{S} \equiv \sqrt{2S+1}$ . The final state  $[[(\Phi_C \chi_C)^{J_C} (\Phi_D \chi_D)^{J_D}]_{J_z}^{J'}] \equiv |\Psi_{\text{final}}^{J'J'_z}\rangle$  of mesons  $C(14)$  and  $D(32)$  can be written in a similar way, so the matrix element on the right-hand side of Eq. (9) is

$$\begin{aligned} \langle \Psi_{\text{final}}^{J'J'_z} | v_r v_s | \Psi_{\text{in}}^{JJ_z} \rangle = \sum_{SLS_z S' L' S'_z} \hat{S} \hat{L} \hat{J}_A \hat{J}_B \begin{Bmatrix} S_A & S_B & S \\ L_A & L_B & L \\ J_A & J_B & J \end{Bmatrix} \hat{S}' \hat{L}' \hat{J}_C \hat{J}_D \begin{Bmatrix} S_C & S_D & S' \\ L_C & L_D & L' \\ J_C & J_D & J' \end{Bmatrix} \\ \times (SS_z L(J_z - S_z) | J J_z) (S' S'_z L'(J'_z - S'_z) | J' J'_z)^* \\ \times \langle (\Phi_C \Phi_D)_{(J'_z - S'_z)}^{L'} | v_r | (\Phi_A \Phi_B)_{(J_z - S_z)}^L \rangle \langle (\chi_C \chi_D)_{S'_z}^{S'} | v_s | (\chi_A \chi_B)_{S_z}^S \rangle. \end{aligned} \quad (11)$$

The above result shows that  $I_{\text{spin-space}}$  is in general a sum of products of a spatial matrix element  $\langle (\Phi_C \Phi_D)_{(J'_z - S'_z)}^{L'} | v_r | (\Phi_A \Phi_B)_{(J_z - S_z)}^L \rangle$  and a spin matrix element  $I_{\text{spin}} = \langle (\chi_C \chi_D)_{S'_z}^{S'} | v_s | (\chi_A \chi_B)_{S_z}^S \rangle$ . For our interaction, the spin matrix element  $\langle (\chi_C \chi_D)_{S'_z}^{S'} | v_s | (\chi_A \chi_B)_{S_z}^S \rangle$  is diagonal in  $S$  and  $S_z$ , and is independent of  $S_z$ , as shown in the next section.

In this paper, we shall specialize to the cases in which mesons  $B, C$ , and  $D$  are all  $S$ -wave mesons with  $L_B = L_C = L_D = 0$ . Therefore we have  $L = L_A, J_B = S_B, J' = S, J'_z = S_z$ , and

$$\langle \Psi_{\text{final}}^{SS_z} | v_r v_s | \Psi_{\text{in}}^{JJ_z} \rangle = \hat{S} \hat{L}_A \hat{J}_A \hat{J}_B \begin{Bmatrix} S_A & S_B & S \\ L_A & 0 & L_A \\ J_A & S_B & J \end{Bmatrix} (SS_z L_A (J_z - S_z) | JJ_z \rangle \langle \Phi_C \Phi_D | v_r | (\Phi_A \Phi_B)_{(J_z - S_z)}^{L_A} \rangle \langle (\chi_C \chi_D)_{S_z}^S | v_s | (\chi_A \chi_B)_{S_z}^S \rangle, \quad (12)$$

where  $|S_A - S_B| \leq S \leq (S_A + S_B)$  and  $|S - L_A| \leq J \leq (S + L_A)$ . For the collision of unpolarized mesons, we can calculate the square of the matrix element,  $|I_{\text{space-spin}}|^2$ , average it over the initial states, and sum it over the final states. The result is

$$\overline{|I_{\text{space-spin}}|^2} = \frac{1}{(2J_A + 1)(2S_B + 1)} \sum_{JJ_z SS_z} (\hat{S} \hat{L}_A \hat{J}_A \hat{J}_B)^2 \begin{Bmatrix} S_A & S_B & S \\ L_A & 0 & L_A \\ J_A & S_B & J \end{Bmatrix}^2 \times |(SS_z L_A (J_z - S_z) | JJ_z \rangle|^2 \left| \sum_i^3 \langle \Phi_C \Phi_D | v_r^{(i)} | (\Phi_A \Phi_B)_{(J_z - S_z)}^{L_A} \rangle \langle (\chi_C \chi_D)_{S_z}^S | v_s^{(i)} | (\chi_A \chi_B)_{S_z}^S \rangle \right|^2. \quad (13)$$

The summation over  $S_z$  can be carried out and the summation over  $J_z$  can be converted to a summation over  $M_A$ . We then obtain

$$\overline{|I_{\text{space-spin}}|^2} = \sum_{SJM_A} (\hat{S} \hat{J})^2 \begin{Bmatrix} S_A & S_B & S \\ L_A & 0 & L_A \\ J_A & S_B & J \end{Bmatrix}^2 \times \left| \sum_i^3 \langle \Phi_C \Phi_D | v_r^{(i)} | (\Phi_A \Phi_B)_{M_A}^{L_A} \rangle \times \langle (\chi_C \chi_D)_{S_z}^S | v_s^{(i)} | (\chi_A \chi_B)_{S_z}^S \rangle \right|^2, \quad (14)$$

where  $-L_A \leq M_A \leq L_A$ . From the relation between the matrix element of  $V_{ij}(r_{ij})$  and the cross section, the above result leads to the following ‘‘unpolarized’’ cross section for the collision of unpolarized mesons:

$$\sigma^{\text{unpol}} = \sum_{SJM_A} (\hat{S} \hat{J})^2 \begin{Bmatrix} S_A & S_B & S \\ L_A & 0 & L_A \\ J_A & S_B & J \end{Bmatrix}^2 \sigma(L_A M_A S S_z), \quad (15)$$

where  $\sigma(L_A M_A S S_z)$  is the cross section for an initial meson with orbital angular momentum  $L_A$  and spin  $S$ , with azimuthal components  $M_A$  and  $S_z$ , respectively. For our interaction of Eq. (2),  $\sigma(L_A M_A S S_z)$  is independent of  $S_z$ , and thus the label  $S_z$  can be omitted. We can write out the results for other simple unpolarized cases. If  $L_A \neq 0$  and  $S_B = 0$ , then  $S = S_A$  and the result of Eq. (15) becomes

$$\sigma^{\text{unpol}} = \frac{1}{(2L_A + 1)} \sum_{M_A = -L_A}^{L_A} \sigma(L_A M_A S_A). \quad (16)$$

If  $L_A = 0$  and  $S_B \neq 0$ , then the result of Eq. (15) is

$$\sigma^{\text{unpol}} = \frac{1}{(2S_A + 1)(2S_B + 1)} \sum_S (2S + 1) \sigma(S), \quad (17)$$

where  $\sigma(S)$  is the cross section when the initial two-meson system has a total spin  $S$ .

## V. EVALUATION OF THE SPIN MATRIX ELEMENT

We denote the spins of the constituents in the scattering process  $A(12)B(34) \rightarrow C(14)D(23)$  by  $s_1, s_2, s_3$ , and  $s_4$ . Using properties of the Wigner  $\{9j\}$  symbol [40], we may rearrange the spins to obtain

$$\begin{aligned} |(\chi_A \chi_B)_{S_z}^S \rangle &= |[(s_1 s_2) S_A (s_3 s_4) S_B]_{S_z}^S \rangle \\ &= (-1)^{S_B - s_4 - s_3} \sum_{S_{14} S_{23}} \hat{S}_A \hat{S}_B \hat{S}_{14} \hat{S}_{23} \\ &\quad \times \begin{Bmatrix} s_1 & s_2 & S_A \\ s_4 & s_3 & S_B \\ S_{14} & S_{23} & S \end{Bmatrix} \\ &\quad \times |[(s_1 s_4) S_{14} (s_2 s_3) S_{23}]_{S_z}^S \rangle. \end{aligned} \quad (18)$$

The phase factor  $(-1)^{S_B - s_4 - s_3}$  arises from an interchange of spins in the Clebsch-Gordon coefficients,

$$|(s_3 s_4) S_B \rangle = (-1)^{S_B - s_4 - s_3} |(s_4 s_3) S_B \rangle. \quad (19)$$

The matrix element of the spin unit operator  $v_s = 1$  is then given by

TABLE I. The values of  $i, j$ , and  $S_{ij}$  in Eq. (21).

Diagram	$i$	$j$	$S_{ij}$
Prior C1	1	4	$S_C$
Prior C2	2	3	$S_D$
Post C1	1	2	$S_A$
Post C2	4	3	$S_B$

$$\begin{aligned}
\langle (\chi_C \chi_D)_{S'_z}^{S'} | v_s | (\chi_A \chi_B)_{S'_z}^S \rangle &= \langle [(s_1 s_4) S_C (s_3 s_2) S_D]_{S'_z}^{S'} | 1 \rangle \\
&\quad \times \langle [(s_1 s_2) S_A (s_3 s_4) S_B]_{S'_z}^S \rangle \\
&= \delta_{SS'} \delta_{S'_z S'_z} (-1)^{S_B + S_D - s_2 - s_4 - 2s_3} \\
&\quad \times \hat{S}_A \hat{S}_B \hat{S}_C \hat{S}_D \\
&\quad \times \begin{Bmatrix} s_1 & s_2 & S_A \\ s_4 & s_3 & S_B \\ S_C & S_D & S \end{Bmatrix}. \quad (20)
\end{aligned}$$

The matrix element of the operator  $v_s = \mathbf{s}_i \cdot \mathbf{s}_j$  can be derived similarly. For diagrams C1 and C2, the matrix element is given by

$$\begin{aligned}
\langle (\chi_C \chi_D)_{S'_z}^{S'} | v_s | (\chi_A \chi_B)_{S'_z}^S \rangle &= \langle [(s_1 s_4) S_C (s_3 s_2) S_D]_{S'_z}^{S'} | \mathbf{s}_i \cdot \mathbf{s}_j | [(s_1 s_2) S_A (s_3 s_4) S_B]_{S'_z}^S \rangle \\
&= \delta_{SS'} \delta_{S'_z S'_z} (-1)^{S_B + S_D - s_2 - s_4 - 2s_3} \hat{S}_A \hat{S}_B \hat{S}_C \hat{S}_D \\
&\quad \times \begin{Bmatrix} s_1 & s_2 & S_A \\ s_4 & s_3 & S_B \\ S_C & S_D & S \end{Bmatrix} \frac{1}{2} [S_{ij}(S_{ij} + 1) \\
&\quad - S_i(S_i + 1) - S_j(S_j + 1)]. \quad (21)
\end{aligned}$$

The values of  $i, j$ , and  $S_{ij}$  for diagrams C1 and C2 are listed in Table I.

The matrix element of  $v_s = \mathbf{s}_i \cdot \mathbf{s}_j$  for diagrams T1 and T2 is somewhat more complicated, and can be shown to be

$$\begin{aligned}
\langle (\chi_C \chi_D)_{S'_z}^{S'} | v_s | (\chi_A \chi_B)_{S'_z}^S \rangle &= \langle [(s_1 s_4) S_C (s_3 s_2) S_D]_{S'_z}^S | \mathbf{s}_i \cdot \mathbf{s}_j | [(s_1 s_2) S_A (s_3 s_4) S_B]_{S'_z}^{S'} \rangle \\
&= \delta_{SS'} \delta_{S'_z S'_z} \sum_{S_{13} S_{24}} (-1)^{S_{24} - s_4 - s_2} (2S_{13} + 1)(2S_{24} + 1) \\
&\quad \times \hat{S}_A \hat{S}_B \hat{S}_C \hat{S}_D \begin{Bmatrix} s_1 & s_2 & S_A \\ s_3 & s_4 & S_B \\ S_{13} & S_{24} & S \end{Bmatrix} \\
&\quad \times \begin{Bmatrix} s_1 & s_4 & S_C \\ s_3 & s_2 & S_D \\ S_{13} & S_{24} & S \end{Bmatrix} \frac{1}{2} [S_{ij}(S_{ij} + 1) \\
&\quad - S_i(S_i + 1) - S_j(S_j + 1)], \quad (22)
\end{aligned}$$

where  $i=1$  and  $j=3$  for diagram T1 and  $i=2$  and  $j=4$  for diagram T2. The quantities  $S_{13}$  and  $S_{24}$  span the full allowed range in this summation.

Equations (20), (21), and (22) give the general result for the spin matrix element  $I_{\text{spin}}$  of the unit operator and the  $\mathbf{s}_i \cdot \mathbf{s}_j$  operator in a rearrangement collision. Our results agree with the explicit coefficients given in Table I of Barnes and Swanson [33].

## VI. EVALUATION OF THE SPATIAL MATRIX ELEMENT

In the quark-interchange reaction of Eq. (1), the masses of the quarks and antiquarks are different in general. Previously, meson scattering calculations with unequal masses using this approach had been discussed in detail in coordinate space [34]. Here we give the corresponding momentum-space results for general quark and antiquark masses.

The spatial matrix element in Eq. (11) is

$$\begin{aligned}
\langle (\Phi_C \Phi_D)_{(J'_z - S'_z)}^{L'} | v_r | (\Phi_A \Phi_B)_{(J_z - S_z)}^L \rangle &= \sum_{M_A M_B M_C M_D} (L_C M_C L_D M_D | L'(J'_z - S'_z)) \\
&\quad \times * (L_A M_A L_B M_B | L(J_z - S_z)) \\
&\quad \times \langle \Phi_C(L_C M_C) \Phi_D(L_D M_D) | v_r | \Phi_A(L_A M_A) \Phi_B(L_B M_B) \rangle. \quad (23)
\end{aligned}$$

TABLE II. Diagram-dependent momentum arguments in post and prior formalisms.

Diagram	$\zeta$	$k_A$	$K_A$	$k_B$	$K_B$	$k_C$	$K_C$	$k_D$	$K_D$
Prior C1	1	$\kappa$	$f_A \mathbf{A}$	$\kappa$	$f_B \mathbf{A} + 2\mathbf{C}$	$\kappa'$	$f_C \mathbf{C}$	$\kappa$	$f_D \mathbf{C} + 2\mathbf{A}$
Prior C2	-1	$\kappa$	$f_A \mathbf{A}$	$\kappa$	$f_B \mathbf{A} - 2\mathbf{C}$	$\kappa$	$-f_C \mathbf{C} + 2\mathbf{A}$	$\kappa'$	$-f_D \mathbf{C}$
Post C1	1	$\kappa$	$f_A \mathbf{A}$	$\kappa'$	$f_B \mathbf{A} + 2\mathbf{C}$	$\kappa'$	$f_C \mathbf{C}$	$\kappa'$	$f_D \mathbf{C} + 2\mathbf{A}$
Post C2	-1	$\kappa$	$f_A \mathbf{A}$	$\kappa'$	$f_B \mathbf{A} - 2\mathbf{C}$	$\kappa$	$-f_C \mathbf{C} + 2\mathbf{A}$	$\kappa$	$-f_D \mathbf{C}$
T1	1	$\kappa$	$f_A \mathbf{A}$	$\kappa'$	$f_B \mathbf{A} + 2\mathbf{C}$	$\kappa'$	$f_C \mathbf{C}$	$\kappa$	$f_D \mathbf{C} + 2\mathbf{A}$
T2	-1	$\kappa$	$f_A \mathbf{A}$	$\kappa'$	$f_B \mathbf{A} - 2\mathbf{C}$	$\kappa$	$-f_C \mathbf{C} + 2\mathbf{A}$	$\kappa'$	$-f_D \mathbf{C}$

For the four diagrams in the reaction  $A + B \rightarrow C + D$  the spatial matrix element

$$I_{\text{space}} = \langle \Phi_C(L_C M_C) \Phi_D(L_D M_D) | v_r | \Phi_A(L_A M_A) \Phi_B(L_B M_B) \rangle \quad (24)$$

can be written in the form

$$I_{\text{space}} = \int \int d\boldsymbol{\kappa} d\boldsymbol{\kappa}' \Phi_A[\zeta(2\mathbf{k}_A - \mathbf{K}_A)] \Phi_B[\zeta(2\mathbf{k}_B - \mathbf{K}_B)] \\ \times \Phi_C[\zeta(2\mathbf{k}_C - \mathbf{K}_C)] \Phi_D[\zeta(2\mathbf{k}_D - \mathbf{K}_D)] V(\boldsymbol{\kappa}' - \boldsymbol{\kappa}). \quad (25)$$

Here the momentum arguments are shown explicitly, and the angular momentum quantum numbers  $L_i$  and  $M_i$  for each meson are implicit. The quantity  $\zeta = \pm 1$  is an overall sign which depends on the diagram (see Table II). The quantity  $V(\mathbf{q})$ , where  $\mathbf{q} = \boldsymbol{\kappa} - \boldsymbol{\kappa}'$ , is the Fourier transform of the interaction  $V_{ij}(r_{ij})$  [the spin and spatial part of  $H_{ij}(r_{ij})$  in Eq. (3)],

$$V(\mathbf{q}) = \int d\mathbf{r}_{ij} e^{-i\mathbf{q} \cdot \mathbf{r}_{ij}} V_{ij}(r_{ij}). \quad (26)$$

The momenta  $\boldsymbol{\kappa}$  is the initial three-momenta of the scattered constituent that is initially in meson  $A$  and  $\boldsymbol{\kappa}'$  is its final three-momenta. The variables  $\{\mathbf{k}_i, (i=A, B, C, D)\}$  are either  $\boldsymbol{\kappa}$  or  $\boldsymbol{\kappa}'$  depending on the diagram, as specified in Table II. We use boldface  $\mathbf{A}$ ,  $\mathbf{B}$ ,  $\mathbf{C}$ , and  $\mathbf{D}$  to represent the momenta of  $A$ ,  $B$ ,  $C$ , and  $D$ , respectively. For simplicity we shall treat the scattering problem in the center-of-mass frame, so that  $\mathbf{B} = -\mathbf{A}$  and  $\mathbf{D} = -\mathbf{C}$ . The quantity  $\{\mathbf{K}_i\}$  is a function of  $\mathbf{A}$ ,  $\mathbf{C}$ , and the mass parameter  $f_i$ , which is a function of the quark and antiquark masses in meson  $i$ . The function  $\mathbf{K}_i(\mathbf{A}, \mathbf{C}, f_i)$  is tabulated for each diagram in Table II. For diagrams T1 and T2, the post and prior variables are identical and so do not need to be tabulated separately.

The mass parameter  $f_i$  is unity for mesons with equal quark and antiquark masses. For unequal masses, the  $\{f_i\}$  are tabulated in Table III in terms of

$$\Delta_i = \frac{m(q)_i - m(\bar{q})_i}{m(q)_i + m(\bar{q})_i}. \quad (27)$$

The  $\{f_i\}$  are the same in post and prior formalisms.

To evaluate the spatial overlap integrals, we expand each meson wave function  $\Phi(2\mathbf{p})$  as a linear combination of (nonorthogonal) Gaussian basis functions  $\phi_n(2\mathbf{p})$  of different widths as

$$\Phi(2\mathbf{p}) = \sum_{n=1}^N a_n \phi_n(2\mathbf{p}), \quad (28)$$

where

$$\phi_n(2\mathbf{p}) = N_n (2p)^l \sqrt{\frac{4\pi}{(2l+1)!!}} Y_{lm}(\hat{\mathbf{p}}) \exp\left\{-\frac{(2\mathbf{p})^2}{8n\beta^2}\right\}. \quad (29)$$

This expansion leads to tractable basis overlap integrals. We choose to normalize the basis function  $\phi_n(2\mathbf{p})$  according to

$$\int d\mathbf{p} |\phi_n(2\mathbf{p})|^2 = 1, \quad (30)$$

which leads to the normalization constant

$$N_n = \left(\frac{1}{\pi n \beta^2}\right)^{3/4} \frac{1}{(2n\beta^2)^{1/2}}. \quad (31)$$

We also normalize the full meson wave function  $\Phi(2\mathbf{p})$  to

$$\int d\mathbf{p} |\Phi(2\mathbf{p})|^2 = 1, \quad (32)$$

which implies a constraint on the coefficients  $\{a_n\}$ .

We shall first present our results for the spatial matrix element, Eq. (25), for the case of all  $S$ -wave mesons, each with a single Gaussian wave function of the type of Eq. (29),

$$\phi_i[\zeta(2\mathbf{k}_i - \mathbf{K}_i)] = N_i \exp\left\{-\frac{\lambda_i}{2}(2\mathbf{k}_i - \mathbf{K}_i)^2\right\}, \quad (33)$$

where  $\lambda_i = 1/4n\beta^2$  and

$$N_i = \sqrt{8} \left(\frac{\lambda_i}{\pi}\right)^{3/4}. \quad (34)$$

The product of the wave functions in Eq. (25) is explicitly

$$\phi_A[\zeta(2\mathbf{k}_A - \mathbf{K}_A)] \phi_B[\zeta(2\mathbf{k}_B - \mathbf{K}_B)] \phi_C \\ \times [\zeta(2\mathbf{k}_C - \mathbf{K}_C)] \phi_D[\zeta(2\mathbf{k}_D - \mathbf{K}_D)] \\ = N_A N_B N_C N_D \exp\left\{-\sum_{i=1}^4 \frac{\lambda_i}{2}(2\mathbf{k}_i - \mathbf{K}_i)^2\right\}. \quad (35)$$

The argument of the exponential, from the product of the four meson wave functions, is a function of  $\mathbf{k}_i = \{\boldsymbol{\kappa}, \boldsymbol{\kappa}'\}$  and the quantities  $\{\mathbf{K}_i\}$ . It can also be written as a function of  $\mathbf{p} = (\boldsymbol{\kappa} + \boldsymbol{\kappa}')/2$  and  $\mathbf{q} = \boldsymbol{\kappa}' - \boldsymbol{\kappa}$ . In terms of  $\mathbf{p}$  and  $\mathbf{q}$ , the  $\{\mathbf{k}_i\}$  are given by

$$\mathbf{k}_i = \mathbf{p} - \eta_i \mathbf{q}/2, \quad (36)$$

where  $\eta_i$  is

$$\eta_i = \begin{cases} +1, & \text{if } \mathbf{k}_i = \boldsymbol{\kappa}, \\ -1, & \text{if } \mathbf{k}_i = \boldsymbol{\kappa}'. \end{cases} \quad (37)$$

Using Eq. (36) and completing the square in the exponential, we obtain

$$\sum_{i=1}^4 \frac{\lambda_i}{2}(2\mathbf{k}_i - \mathbf{K}_i)^2 = 2 \sum_i^4 \lambda_i (\mathbf{p} - \mathbf{p}_0)^2 + \frac{\mu}{2} (\mathbf{q} - \mathbf{q}_0)^2 + \frac{\nu}{2}, \quad (38)$$

where the quantities  $\mathbf{p}_0$ ,  $\mathbf{q}_0$ ,  $\mu$ , and  $\nu$  are defined below. The shift  $\mathbf{p}_0$  is

TABLE III. The mass parameters  $f_i$  for each diagram.

Diagram =	C1	C2	T1	T2
$f_A =$	$1 + \Delta_A$	$1 - \Delta_A$	$1 + \Delta_A$	$1 - \Delta_A$
$f_B =$	$1 - \Delta_B$	$1 + \Delta_B$	$1 - \Delta_B$	$1 + \Delta_B$
$f_C =$	$1 + \Delta_C$	$1 + \Delta_C$	$1 + \Delta_C$	$1 + \Delta_C$
$f_D =$	$1 - \Delta_D$	$1 - \Delta_D$	$1 - \Delta_D$	$1 - \Delta_D$

$$\mathbf{p}_0 = r_0 \mathbf{q} + \mathbf{s}_0, \quad (39)$$

where  $r_0$  and  $\mathbf{s}_0$  are

$$r_0 = \frac{\sum_{i=1}^4 \eta_i \lambda_i}{2 \sum_{i=1}^4 \lambda_i}, \quad (40)$$

$$\mathbf{s}_0 = \frac{\sum_{i=1}^4 \eta_i \mathbf{K}_i}{2 \sum_{i=1}^4 \lambda_i}. \quad (41)$$

The quantity  $\mu$  in Eq. (38) is

$$\mu = 4 \left( \sum_{i=1}^4 \frac{1 + \eta_i}{2} \lambda_i \right) \left( \sum_{j=1}^4 \frac{1 - \eta_j}{2} \lambda_j \right) / \sum_{i=1}^4 \lambda_i, \quad (42)$$

the shift  $\mathbf{q}_0$  is

$$\mathbf{q}_0 = - \frac{2}{\mu \sum_{i=1}^4 \lambda_i} \left[ \left( \sum_{i=1}^4 \frac{1 - \eta_i}{2} \lambda_i \right) \left( \sum_{j=1}^4 \frac{1 + \eta_j}{2} \lambda_j \mathbf{K}_j \right) - \left( \sum_{i=1}^4 \frac{1 + \eta_i}{2} \lambda_i \right) \left( \sum_{j=1}^4 \frac{1 - \eta_j}{2} \lambda_j \mathbf{K}_j \right) \right], \quad (43)$$

and  $\nu$  is

$$\nu = \sum_{i=1}^4 \lambda_i \mathbf{K}_i^2 - 4 \sum_{i=1}^4 \lambda_i \mathbf{s}_0^2 - \mu \mathbf{q}_0^2. \quad (44)$$

The product of the wave functions in Eq. (25) can therefore be written in a shifted Gaussian form

$$\begin{aligned} & \phi_A[\zeta(2\mathbf{k}_A - \mathbf{K}_A)] \phi_B[\zeta(2\mathbf{k}_B - \mathbf{K}_B)] \phi_C[\zeta(2\mathbf{k}_C - \mathbf{K}_C)] \\ & \times \phi_D[\zeta(2\mathbf{k}_D - \mathbf{K}_D)] \\ & = N_A N_B N_C N_D \exp \left\{ -2 \sum_{i=1}^4 \lambda_i (\mathbf{p} - \mathbf{p}_0)^2 \right. \\ & \left. - \frac{\mu}{2} (\mathbf{q} - \mathbf{q}_0)^2 - \frac{\nu}{2} \right\}. \end{aligned} \quad (45)$$

The spatial matrix element of Eq. (25) then becomes

$$\begin{aligned} & \int \int d\boldsymbol{\kappa} d\boldsymbol{\kappa}' \phi_A[\zeta(2\mathbf{k}_A - \mathbf{K}_A)] \phi_B[\zeta(2\mathbf{k}_B - \mathbf{K}_B)] \\ & \times \phi_C[\zeta(2\mathbf{k}_C - \mathbf{K}_C)] \phi_D[\zeta(2\mathbf{k}_D - \mathbf{K}_D)] V(\mathbf{q}) \\ & = \int \int d\mathbf{p} d\mathbf{q} N_A N_B N_C N_D \\ & \times \exp \left\{ -2 \sum_{i=1}^4 \lambda_i (\mathbf{p} - \mathbf{p}_0)^2 - \frac{\mu}{2} (\mathbf{q} - \mathbf{q}_0)^2 - \frac{\nu}{2} \right\} V(\mathbf{q}). \end{aligned} \quad (46)$$

The integration over  $\mathbf{p}$  can be carried out analytically, which gives

$$\begin{aligned} & \int \int d\mathbf{p} d\mathbf{q} \prod_{i=1}^4 \phi_i[\zeta(2\mathbf{k}_i - \mathbf{K}_i)] V(\mathbf{q}) \\ & = N_A N_B N_C N_D \left( \frac{\pi}{2 \sum_{i=1}^4 \lambda_i^4} \right)^{3/2} \\ & \times e^{-\nu/2} \int d\mathbf{q} e^{-\mu(\mathbf{q} - \mathbf{q}_0)^2/2} V(\mathbf{q}). \end{aligned} \quad (47)$$

Thus, the six-dimensional integral of Eq. (46) is simplified to a three-dimensional integral involving an integration over  $V(\mathbf{q})$ .

The interaction  $V(\mathbf{q})$  is the Fourier transform of the standard quark model  $V_{ij}(r)$ . We need the matrix elements for the color-Coulomb, spin-spin, and linear confinement interactions, and we have (using some integrals of Ref. [38])

$$\begin{aligned} & \int d\mathbf{q} e^{-\mu(\mathbf{q} - \mathbf{q}_0)^2/2} V_{\text{Cou}}(\mathbf{q}) \\ & = \int d\mathbf{q} e^{-\mu(\mathbf{q} - \mathbf{q}_0)^2/2} \frac{4\pi\alpha_s}{\mathbf{q}^2} \\ & = \frac{4\pi\alpha_s (2\pi)^{3/2}}{\sqrt{\mu}} e^{-\mu\mathbf{q}_0^2/2} {}_1F_1 \left( \frac{1}{2}, \frac{3}{2}, \frac{\mu\mathbf{q}_0^2}{2} \right), \end{aligned} \quad (48)$$

$$\begin{aligned} & \int d\mathbf{q} e^{-\mu(\mathbf{q} - \mathbf{q}_0)^2/2} V_{\text{ss}}(\mathbf{q}) \\ & = \int d\mathbf{q} e^{-\mu(\mathbf{q} - \mathbf{q}_0)^2/2} \left( \frac{-8\pi\alpha_s}{3m_i m_j} \right) e^{-\mathbf{q}^2/4\sigma^2} \\ & = \frac{-8\pi\alpha_s}{3m_i m_j} \left( \frac{2\pi}{\mu} \right)^{3/2} \left( \frac{2\sigma^2\mu}{1 + 2\sigma^2\mu} \right)^{3/2} \\ & \times \exp \left\{ - \frac{\mu\mathbf{q}_0^2}{2(1 + 2\sigma^2\mu)} \right\}, \end{aligned} \quad (49)$$

and

$$\int d\mathbf{q} e^{-\mu(\mathbf{q}-\mathbf{q}_0)^2/2} V_{\text{lin}}(\mathbf{q})$$

$$= \left(-\frac{3}{4}\right) 8\pi b \left(\frac{2\pi}{3}\right)^{3/2} \mu^2 e^{-\mu q_0^2/2} {}_1F_1\left(-\frac{1}{2}, \frac{3}{2}, \frac{\mu q_0^2}{2}\right),$$
(50)

where  $V_{\text{lin}}(\mathbf{q}) = (-3/4) \int d\mathbf{r} e^{-i\mathbf{q}\cdot\mathbf{r}} br$ . These results allow one to evaluate the transition matrix elements  $T_{fi}$  explicitly for the different interactions in diagrams C1, C2, T1, and T2 for the case of Gaussian meson wave functions.

The wave functions we employ here are in general sums of Gaussians of different widths [Eq. (28)]. Equation (25) can be evaluated in that case as well, so that the spatial matrix element Eq. (25) becomes

$$I_{\text{space}} = \int \int d\mathbf{k} d\mathbf{k}' \Phi_A[\zeta(2\mathbf{k}_A - \mathbf{K}_A)] \Phi_B[\zeta(2\mathbf{k}_B - \mathbf{K}_B)] \Phi_C[\zeta(2\mathbf{k}_C - \mathbf{K}_C)] \Phi_D[\zeta(2\mathbf{k}_D - \mathbf{K}_D)] V(\mathbf{k}' - \mathbf{k})$$

$$= \sum_{n_A=1}^N \sum_{n_B=1}^N \sum_{n_C=1}^N \sum_{n_D=1}^N a_{n_A} a_{n_B} a_{n_C} a_{n_D} I_{\text{space}}(n_A, n_B, n_C, n_D),$$
(51)

where

$$I_{\text{space}}(n_A, n_B, n_C, n_D) = \int \int d\mathbf{k} d\mathbf{k}' \phi_{A n_A}[\zeta(2\mathbf{k}_A - \mathbf{K}_A)] \phi_{B n_B}[\zeta(2\mathbf{k}_B - \mathbf{K}_B)]$$

$$\times \phi_{C n_C}[\zeta(2\mathbf{k}_C - \mathbf{K}_C)] \phi_{D n_D}[\zeta(2\mathbf{k}_D - \mathbf{K}_D)] V(\mathbf{k}' - \mathbf{k}).$$
(52)

$I_{\text{space}}(n_A, n_B, n_C, n_D)$  is the previous result of Eq. (25) for a single-component wave function. The overlap integral in the multicomponent case is simply a sum of single-component contributions, each weighed by a coefficient product  $a_{n_A} a_{n_B} a_{n_C} a_{n_D}$ .

After the matrix elements for the interaction (2) are evaluated, the cross section for the process  $A+B \rightarrow C+D$  can then be obtained using conventional scattering theory, as discussed in Sec. II.

## VII. EVALUATION OF THE SPATIAL MATRIX ELEMENT FOR AN $L=1$ MESON

In the last section, we considered the scattering of  $S$ -wave ( $L=0$ ) mesons. Here we generalize to collisions in which a  $P$ -wave ( $L=1$ ) meson  $A$  collides with an  $S$ -wave meson  $B$ , and scatter into two  $S$ -wave mesons  $C$  and  $D$ .

First we consider single-component Gaussian wave functions. (The results can be easily generalized to multicomponent Gaussian wave functions.) Equation (25) becomes

$$\int \int d\mathbf{k} d\mathbf{k}' \phi_A(2\mathbf{k}_A - \mathbf{K}_A) \phi_B(2\mathbf{k}_B - \mathbf{K}_B) \phi_C(2\mathbf{k}_C - \mathbf{K}_C) \phi_D(2\mathbf{k}_D - \mathbf{K}_D) V(\mathbf{q})$$

$$= \int \int d\mathbf{k} d\mathbf{k}' N_A |2\mathbf{p}_A|^{L_A} \sqrt{\frac{4\pi}{(2L_A+1)!!}} Y_{L_A M_A}(\hat{\mathbf{p}}_A) \exp\left\{-\frac{\lambda_i}{2}(2\mathbf{k}_A - \mathbf{K}_A)^2\right\}$$

$$\times \phi_B(2\mathbf{k}_B - \mathbf{K}_B) \phi_C(2\mathbf{k}_C - \mathbf{K}_C) \phi_D(2\mathbf{k}_D - \mathbf{K}_D) V(\mathbf{q}),$$

where  $2\mathbf{p}_A = 2\mathbf{k}_A - \mathbf{K}_A$ . Setting  $L_A = 1$  for the  $P$ -wave meson  $A$ , we have

$$|2\mathbf{k}_A - \mathbf{K}_A|^{L_A} \sqrt{\frac{4\pi}{(2L_A+1)!!}} Y_{L_A M_A}(\hat{\mathbf{p}}_A) = \begin{cases} 2\kappa_z - f_A A_z & \text{if } M_A = 0, \\ -(2\kappa_x - f_A A_x) - i(2\kappa_y - f_A A_y) & \text{if } M_A = 1, \\ (2\kappa_x - f_A A_x) - i(2\kappa_y - f_A A_y) & \text{if } M_A = -1. \end{cases}$$
(53)

It then suffices to evaluate

$$\begin{aligned}
& \int \int d\boldsymbol{\kappa} d\boldsymbol{\kappa}' (2\boldsymbol{\kappa} - f_A \mathbf{A})_k N_A \exp\left\{-\frac{\lambda_A}{2}(2\mathbf{k}_A - \mathbf{K}_A)^2\right\} \phi_B(2\mathbf{k}_B - \mathbf{K}_B) \phi_C(2\mathbf{k}_C - \mathbf{K}_C) \phi_D(2\mathbf{k}_D - \mathbf{K}_D) V(\mathbf{q}) \\
& = \int \int d\mathbf{p} d\mathbf{q} (2\boldsymbol{\kappa} - f_A \mathbf{A})_k N_A N_B N_C N_D \exp\left\{-2\sum_{i=1}^4 \lambda_i (\mathbf{p} - \mathbf{p}_0)^2 - \frac{\mu}{2}(\mathbf{q} - \mathbf{q}_0)^2 - \frac{\nu}{2}\right\} V(\mathbf{q}).
\end{aligned} \tag{54}$$

We can express  $2\boldsymbol{\kappa} - f_A \mathbf{A}$  in terms of  $\mathbf{p}$  and  $\mathbf{q}$ :

$$2\boldsymbol{\kappa} - f_A \mathbf{A} = 2\mathbf{p} - \mathbf{q} - f_A \mathbf{A} = 2(\mathbf{p} - \mathbf{p}_0) + 2\mathbf{p}_0 - \mathbf{q} - f_A \mathbf{A}. \tag{55}$$

Substituting Eq. (39) into this result, we find

$$2\boldsymbol{\kappa} - f_A \mathbf{A} = 2(\mathbf{p} - \mathbf{p}_0) + (2r_0 - 1)(\mathbf{q} - \mathbf{q}_0) + (2r_0 - 1)\mathbf{q}_0 + 2\mathbf{s}_0 - f_A \mathbf{A}. \tag{56}$$

The integral of  $\mathbf{p} - \mathbf{p}_0$  gives zero. The integration over the last three terms can be carried out in the same way as in the  $L_A = 0$  case, because  $\mathbf{q}_0$ ,  $\mathbf{s}_0$ , and  $\mathbf{A}$  are independent of the integration variables. It is thus only necessary to evaluate the integral

$$\int \int d\mathbf{p} d\mathbf{q} N_A N_B N_C N_D (\mathbf{q} - \mathbf{q}_0)_k \exp\left\{-2\sum_{i=1}^4 \lambda_i (\mathbf{p} - \mathbf{p}_0)^2 - \frac{\mu}{2}(\mathbf{q} - \mathbf{q}_0)^2 - \frac{\nu}{2}\right\} V(\mathbf{q}). \tag{57}$$

The integration over  $\mathbf{p}$  can be carried out analytically, which gives

$$\begin{aligned}
& \int \int d\mathbf{p} d\mathbf{q} N_A N_B N_C N_D (\mathbf{q} - \mathbf{q}_0)_k \exp\left\{-2\sum_{i=1}^4 \lambda_i (\mathbf{p} - \mathbf{p}_0)^2 - \frac{\mu}{2}(\mathbf{q} - \mathbf{q}_0)^2 - \frac{\nu}{2}\right\} V(\mathbf{q}) \\
& = N_A N_B N_C N_D \left(\frac{\pi}{2}\sum_{i=1}^4 \lambda_i^4\right)^{3/2} e^{-\nu/2} \frac{1}{\mu} \frac{\partial}{\partial q_{0k}} \int d\mathbf{q} e^{-\mu(\mathbf{q} - \mathbf{q}_0)^2/2} V(\mathbf{q}).
\end{aligned} \tag{58}$$

The  $d\mathbf{q}$  integrals for the various potentials have already been obtained in closed form, and the differentiation with respect to  $q_{0k}$  is straightforward. We then find

$$\frac{\partial}{\partial q_{0k}} \int d\mathbf{q} e^{-\mu(\mathbf{q} - \mathbf{q}_0)^2/2} V_{\text{Coul}}(\mathbf{q}) = \frac{4\pi\alpha_s (2\pi)^{3/2}}{\sqrt{\mu}} e^{-\mu q_0^2/2} \left[ -{}_1F_1\left(\frac{1}{2}, \frac{3}{2}, \frac{\mu q_0^2}{2}\right) + \frac{1}{3} {}_1F_1\left(\frac{3}{2}, \frac{5}{2}, \frac{\mu q_0^2}{2}\right) \right] \mu q_{0k}, \tag{59}$$

$$\frac{\partial}{\partial q_{0k}} \int d\mathbf{q} e^{-\mu(\mathbf{q} - \mathbf{q}_0)^2/2} V_{\text{ss}}(\mathbf{q}) = \frac{-8\pi\alpha_s}{3m_i m_j} \left(\frac{2\pi}{\mu}\right)^{3/2} \left(\frac{2\sigma^2\mu}{1+2\sigma^2\mu}\right)^{3/2} \exp\left\{-\frac{\mu q_0^2}{2(1+2\sigma^2\mu)}\right\} \left(-\frac{\mu q_{0i}}{1+2\sigma^2\mu}\right), \tag{60}$$

and

$$\frac{\partial}{\partial q_{0k}} \int d\mathbf{q} e^{-\mu(\mathbf{q} - \mathbf{q}_0)^2/2} V_{\text{lin}}(\mathbf{q}) = \left(-\frac{3}{4}\right) b \ 8\pi \left(\frac{2\pi}{3}\right)^{3/2} \mu^2 e^{-\mu q_0^2/2} \left[ -{}_1F_1\left(-\frac{1}{2}, \frac{3}{2}, \frac{\mu q_0^2}{2}\right) - \frac{1}{3} {}_1F_1\left(\frac{1}{2}, \frac{5}{2}, \frac{\mu q_0^2}{2}\right) \right] \mu q_{0k}. \tag{61}$$

The scattering amplitude  $T_{fi}$  and cross section  $\sigma_{fi}$  for the dissociation of a  $P$ -wave meson through an  $SP \rightarrow SS$  reaction will subsequently be evaluated using these results.

### VIII. MESON WAVE FUNCTIONS

In nonrelativistic reaction theory, the equality of the scattering amplitude for rearrangement reactions in post and prior formalisms follows if and only if the two-body interaction used in evaluating the scattering matrix elements is identical to the interaction that generates the bound-state wave functions. If this is not the case, the post and prior scattering amplitudes will differ in general. It is therefore especially important to determine accurate bound-state wave functions in evaluating scattering amplitudes. For this purpose, we will first search for a set of interaction Hamiltonian parameters that fit the known meson spectrum with reasonable accuracy. This interaction and the associated bound-state wave functions will be used in our subsequent reaction calculations.

For a bound state of quark  $i$  and antiquark  $j$  of momentum  $\mathbf{p}_i$  and  $\mathbf{p}_j$  and reduced momentum  $\mathbf{p}$ ,

$$\mathbf{p} = \frac{m_j \mathbf{p}_i - m_i \mathbf{p}_j}{m_i + m_j}, \quad (62)$$

the Hamiltonian is

$$H = \frac{\mathbf{p}^2}{2\mu} + V(r), \quad (63)$$

where  $\mu$  is the reduced mass  $m_i m_j / (m_i + m_j)$ , and  $V(r)$  is the quark-antiquark interaction [see  $H_{ij}$  of Eq. (2)],

$$V(r) = -\frac{\boldsymbol{\lambda}(i) \cdot \boldsymbol{\lambda}^T(j)}{2} \left\{ \frac{\alpha_s}{r} - \frac{3b}{4} r \right. \\ \left. - \frac{8\pi\alpha_s}{3m_i m_j} \mathbf{s}_i \cdot \mathbf{s}_j \left( \frac{\boldsymbol{\sigma}^3}{\pi^{3/2}} \right) e^{-\sigma^2 r^2} + V_{\text{con}} \right\}. \quad (64)$$

For a quark and antiquark in a color-singlet hadron, the matrix element of  $-\boldsymbol{\lambda}(i) \cdot \boldsymbol{\lambda}^T(j)/4$  is the familiar color factor  $C_f = -4/3$ .

For given orbital angular momentum quantum numbers  $l$  and  $m$ , the eigenstate  $\Phi(2\mathbf{p})$  of this Hamiltonian can be represented using the expansion in Eq. (28) in the set of (non-orthogonal) Gaussian basis states  $\{\phi_n\}$  of Eq. (29) with expansion coefficients  $\{a_n\}$ . The eigenvalue equation  $H\Phi = E\Phi$  then becomes the matrix equation

$$\mathcal{H}a = EBa, \quad (65)$$

where  $a$  is a column matrix with elements  $\{a_1, a_2, \dots, a_N\}$ ,  $B$  is the symmetric matrix

$$B_{ij} = \langle i|j \rangle \equiv \int d\mathbf{p} \phi_i^*(2\mathbf{p}) \phi_j(2\mathbf{p}) = \left( 2 \sqrt{\frac{ij}{i+j}} \right)^{l+3/2}, \quad (66)$$

and  $\mathcal{H}$  is the Hamiltonian matrix

$$\mathcal{H}_{ij} = T_{ij} + V_{ij}, \quad (67)$$

which is the sum of the kinetic energy matrix  $T_{ij}$ ,

$$T_{ij} = \int d\mathbf{p} \phi_i^*(2\mathbf{p}) \frac{\mathbf{p}^2}{2\mu} \phi_j(2\mathbf{p}) \\ = (2l+3) \frac{ij}{i+j} \left( 2 \sqrt{\frac{ij}{i+j}} \right)^{l+3/2} \frac{\beta^2}{2\mu} \quad (68)$$

and the potential matrix  $V_{ij}$ ,

$$V_{ij} \equiv \langle i|V|j \rangle = (2\pi)^3 \int d\mathbf{r} \tilde{\phi}_i^*(\mathbf{r}) V(\mathbf{r}) \tilde{\phi}_j(\mathbf{r}), \quad (69)$$

where  $\tilde{\phi}_i(\mathbf{r})$  is the Fourier transform of  $\phi_i(2\mathbf{p})$ ,

$$\tilde{\phi}_i(\mathbf{r}) = \int \frac{d\mathbf{p}}{(2\pi)^3} e^{i\mathbf{p} \cdot \mathbf{r}} \phi_i(2\mathbf{p}). \quad (70)$$

Evaluation of the potential matrix elements for the color-Coulomb interaction gives

$$V_{ij}(\text{Cou.}) = C_f \alpha_s \left\langle i \left| \frac{1}{r} \right| j \right\rangle \\ = C_f \frac{\alpha_s \beta}{(2\pi)^{3/2}} \frac{2^l l!}{(2l+1)!!} \sqrt{i+j} \left( 2 \sqrt{\frac{ij}{i+j}} \right)^{l+3/2}. \quad (71)$$

For the linear interaction we similarly find

$$V_{ij}(\text{lin.}) = \left\langle i \left| C_f \left( -\frac{3}{4} \right) b r \right| j \right\rangle \\ = C_f \left( -\frac{3}{4} \right) \frac{b}{\beta} \frac{8\pi}{(2\pi)^{3/2}} \frac{(l+1)!}{(2l+1)!!} \\ \times \frac{1}{\sqrt{i+j}} \left( 2 \sqrt{\frac{ij}{i+j}} \right)^{l+3/2}, \quad (72)$$

and for the spin-spin interaction we find

$$V_{ij}(\text{ss}) = -C_f \frac{8\pi\alpha_s}{3m_i m_j} \left( \frac{\boldsymbol{\sigma}^3}{\pi^{3/2}} \right) \langle i | \mathbf{s}_i \cdot \mathbf{s}_j e^{-\sigma^2 r^2} | j \rangle \\ = -C_f \frac{8\pi\alpha_s}{3m_i m_j} \mathbf{s}_i \cdot \mathbf{s}_j \left( \frac{\boldsymbol{\sigma}^3}{\pi^{3/2}} \right) \\ \times \left( 2 \sqrt{\frac{ij}{i+j+2\sigma^2/\beta^2}} \right)^{l+3/2}. \quad (73)$$

Given these Hamiltonian matrix elements, the eigenvalues and eigenvectors can be obtained from the eigenvalue equation (65). In our numerical calculations we used a six-component ( $N=6$ ) space of Gaussian basis functions.

For this study we assumed a running coupling constant combined with an otherwise fairly conventional quark model parameter set, given by

$$\alpha_s(Q^2) = \frac{12\pi}{(33-2n_f)\ln(A+Q^2/B^2)},$$

$$A = 10, \quad B = 0.31 \text{ GeV},$$

$$b = 0.18 \text{ GeV}^2, \quad \sigma = 0.897 \text{ GeV},$$

$$m_u = m_d = 0.334 \text{ GeV},$$

$$m_s = 0.575 \text{ GeV}, \quad m_c = 1.776 \text{ GeV}, \quad m_b = 5.102 \text{ GeV},$$

$$V_{\text{con}} = -0.620 \text{ GeV}. \quad (74)$$

We identified the scale  $Q^2$  in the running coupling constant with the square of the invariant mass of the interacting constituents,  $Q^2 = s_{ij}$ . This set of parameters leads to a meson spectrum which is reasonably close to experiment (see Fig. 3); the theoretical masses and wave functions are given in Appendix A. The parameter set used earlier in [21] is similar to this set but it has a fixed strong-coupling constant. An alternative set of quark model parameters, without a running coupling constant, was used for comparison. This second set was  $\alpha_s = 0.594$ ,  $b = 0.162 \text{ GeV}^2$ ,  $\sigma = 0.897 \text{ GeV}$ ,  $m_u = m_d = 0.335 \text{ GeV}$ , and  $m_c = 1.6 \text{ GeV}$  and a flavor-dependent  $V_{\text{con}}$ .

Having obtained the set of coefficients  $\{a_n\}$  for each initial and final meson, we can proceed to the calculation of the scattering amplitudes  $T_{fi}$  and the dissociation cross sections  $\sigma_{fi}$ . Some explanation of the evaluation of our (somewhat arbitrary) choice of momentum scale  $Q^2 = s_{ij}$  in the running coupling constant  $\alpha(Q^2)$  in Eq. (74) for the scattering problem is appropriate. For a reaction process involving the interaction of constituent  $i=a$  in meson  $A(aa')$  with  $j=b$  in meson  $B(bb')$ , we can determine the invariant mass squared  $s_{ij}$  of  $a$  and  $b$  as follows: Constituent  $a$  carries a fraction  $x_+$  of the forward light-cone momentum of the initial meson  $A$ , and  $b$  carries a fraction  $x_-$  of the backward light-cone momentum of initial meson  $B$ . For simplicity, we assume that the momentum fraction carried by a constituent is proportional to its rest mass, which is exact in the weak binding limit:

$$x_+ = \frac{m_a}{m_a + m_{a'}}, \quad (75)$$

$$x_- = \frac{m_b}{m_b + m_{b'}}. \quad (76)$$

Assuming also that constituents  $a$  and  $b$  are on mass shell, their momenta are [2]

$$\begin{pmatrix} a_0 \\ a_z \end{pmatrix} = \frac{1}{2} \left[ x_+(A_0 + A_z) \pm \frac{m_a^2}{x_+(A_0 + A_z)} \right] \quad (77)$$

and

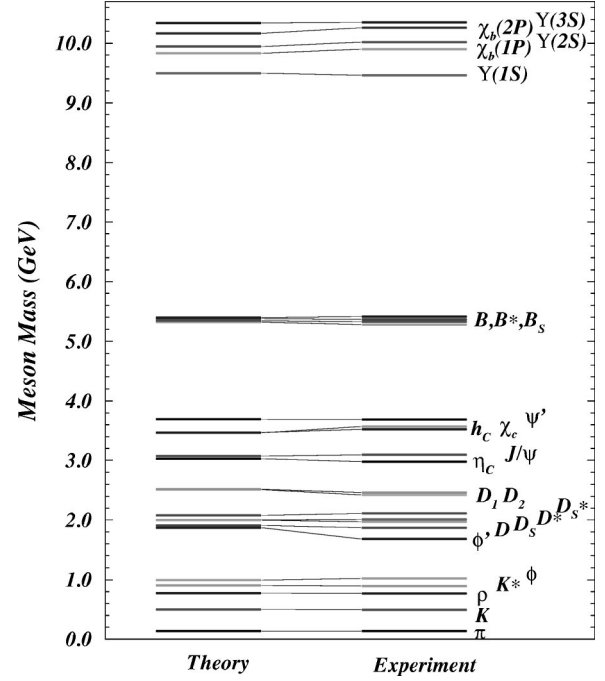


FIG. 3. Comparison of experimental energy levels and theoretical energy levels calculated with the parameter set of Eq. (74).

$$\begin{pmatrix} b_0 \\ -b_z \end{pmatrix} = \frac{1}{2} \left[ x_-(B_0 - B_z) \pm \frac{m_b^2}{x_-(B_0 - B_z)} \right], \quad (78)$$

and the invariant mass of  $a$  and  $b$  is then given by

$$s_{ab} = (a+b)^2 = (a_0 + b_0)^2 - (a_z + b_z)^2. \quad (79)$$

We identify this with the argument  $Q^2$  of the running coupling constant  $\alpha_s(Q^2)$  in Eq. (74).

In Fig. 4 we show a test of the accuracy of this scattering model with experimental data in an analogous low-energy reaction,  $I = 2\pi\pi$  scattering. The prediction for the dominant  $S$ -wave phase shift is shown together with the data of Hoogland *et al.* [41]. Note that this is *not* a fit; all the parameters are determined by meson spectroscopy, which fixes the interquark forces and wave functions that are then used to calculate the meson-meson scattering amplitude.

## IX. TEST OF POST-PRIOR EQUIVALENCE IN $\pi + J/\psi$ DISSOCIATION

In nonrelativistic scattering theory the post and prior results can be formally proved to be equivalent, so that the two theoretical cross sections are indeed identical. This proof requires that the interaction  $V$  used to determine the external meson wave functions be identical to the interaction used in the evaluation of the scattering amplitude. Numerical confirmation of this post-prior equivalence constitutes a very non-trivial test of the accuracy of the numerical procedures used both in determining the bound-state wave function and in evaluating the complete meson-meson scattering amplitude [34].

To test post-prior equivalence in our  $J/\psi$  dissociation cal-

culations (in the nonrelativistic formalism), we have carried out the evaluation of the cross section using both post and prior formalisms. Of necessity we assumed nonrelativistic kinematics and theoretical masses to determine the external meson momenta  $|A|$  and  $|C|$ , which appear in the overlap integrals. The post-prior equivalence holds if the coupling constant does not depend on energy. We are well advised to use a set of parameters with a fixed running coupling constant  $\alpha_s$  for this test. We used therefore the parameter set [21]  $\alpha_s = 0.58$ ,  $b = 0.18 \text{ GeV}^2$ ,  $\sigma = 0.897 \text{ GeV}$ ,  $m_{u,d} = 0.345 \text{ GeV}$ ,  $m_c = 1.931 \text{ GeV}$ , and  $V_{\text{con}} = -0.612 \text{ GeV}$ , which are close to standard values and were chosen because they reproduce the physical masses of the  $\pi$ ,  $D$ ,  $D^*$ ,  $J/\psi$ , and  $\psi'$  rather well. Figure 5(a) shows the dissociation cross sections for  $\pi + \psi$  collisions as a function of the initial kinetic energy  $E_{KE}$  measured in the center-of-mass frame, defined as  $E_{KE} = \sqrt{s} - m_A - m_B$  where  $m_A$  and  $m_B$  are the masses of the incident mesons. The differences between the post and prior results in Fig. 5(a) are indeed rather small, which confirms post-prior equivalence assuming nonrelativistic dynamics. (The residual discrepancy is mainly due to our use of a truncated basis in expanding the meson wave functions.) Figure 5(b) shows the corresponding results for  $\pi + \psi'$  dissociation. In this case there is greater sensitivity to the approximate  $\psi'$  wave function, due to large cancellations in the numerical integration of a radially excited wave function.

In the comparisons shown in Fig. 5 we have used theoretical masses for the mesons; the proof of post-prior equivalence makes use of the theoretical bound-state masses from the Schrödinger equation with the given potential, rather than the experimental ones. Our theoretical masses are close to experiment but are not exact, as is evident in Fig. 3. If one instead assumes experimental values for the meson masses, there will be additional post-prior discrepancies in our cross section calculations. In our subsequent cross section calculations we do assume experimental masses in order to reproduce correct thresholds; the consequence is a systematic uncertainty in the cross sections which may be estimated by comparing post and prior predictions.

It should be noted that post-prior equivalence had only been proven for bound-state scattering in nonrelativistic quantum mechanics [39]. Recently an extension of this proof to scattering in a relativistic generalization of quantum mechanics was given by Wong and Crater [42], using Dirac's constraint dynamics. A full relativistic treatment of this problem will involve the derivation of relativistic two-body wave functions and Wigner spin rotations, which is beyond the scope of the present investigation. We will adopt an intermediate approach and assume relativistic kinematics for the initial and final mesons and use relativistic phase space; in consequence we find different "post" and "prior" cross sections in general. Here we will take the mean value of the post and prior results as our estimated cross section; separate post and prior cross sections will be shown as an indication of our systematic uncertainty.

## X. CROSS SECTIONS FOR $J/\psi$ AND $\psi'$ DISSOCIATION

Depending on the incident energies, dissociation of the  $J/\psi$  and  $\psi'$  by pions can lead to many different exclusive

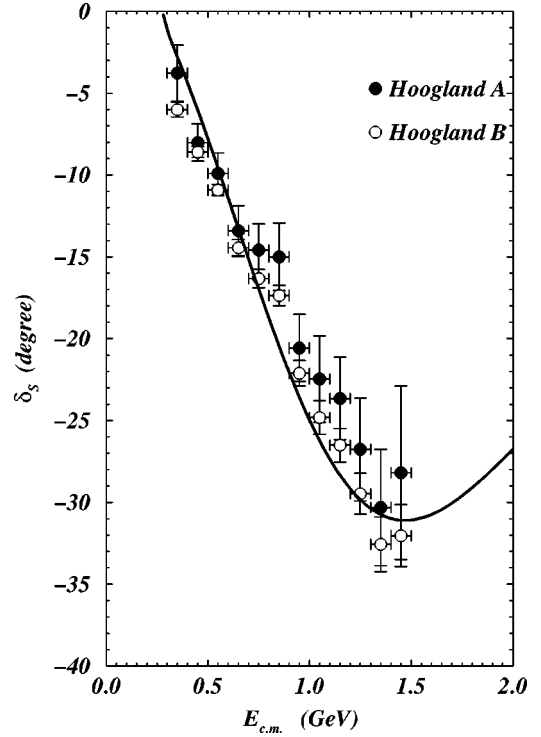


FIG. 4. Comparison of our theoretical  $I=2 \pi\pi$  phase shift (solid curve) with the data of Hoogland *et al.* [41].

final states. There are several selection rules that eliminate or suppress many of the *a priori* possible final channels, given our simple quark-model Hamiltonian and Born-order scattering amplitudes. Considerable simplification follows from the fact that our model Hamiltonian conserves total spin  $S_{tot}$  in the quark-interchange model, as one can easily see from Eqs. (11), (20), (21), and (22). Since the  $J/\psi$  and  $\psi'$  have  $S=1$  and pions have  $S=0$ , the initial and final states in  $\pi + J/\psi$  and  $\pi + \psi'$  collisions must both have  $S_{tot}=1$ ; this forbids  $D\bar{D}$  final states. With increasing invariant mass we next encounter the final states  $D\bar{D}^*$ ,  $D^*\bar{D}$ , and  $D^*\bar{D}^*$ . In Fig. 6 we show the exclusive dissociation cross sections for  $\pi + J/\psi$  and  $\pi + \psi'$  collisions into these first few allowed final states. The total dissociation cross section, which is the sum of the exclusive cross sections, is shown as a solid line. Our estimate is the mean of the total post and prior cross sections, which are also shown in Fig. 6. The estimated range of uncertainty, due to the post-prior discrepancy and to parameter variations, is shown as a shaded band.

The  $J/\psi$  dissociation processes  $\pi + J/\psi \rightarrow D^*\bar{D}$  and  $D\bar{D}^*$  have a threshold of about  $E_{KE} = 0.65 \text{ GeV}$ , and the total dissociation cross section reaches approximately 1 mb not far above threshold [Fig. 6(a)]. This  $\pi + J/\psi$  cross section is considerably smaller than the peak value of about 7 mb found by Martins *et al.* [20], largely due to their assumption of a color-independent confining interaction.

The threshold for  $\pi + \psi' \rightarrow D\bar{D}^* + D^*\bar{D}$  is only about  $E_{KE} = 0.05 \text{ GeV}$ , and in consequence the  $\psi'$  cross sections are much larger near threshold. The total  $\pi + \psi'$  dissociation cross section has maxima of  $\approx 4.2(0.5) \text{ mb}$  and  $\approx 2.8(0.5) \text{ mb}$  at  $E_{KE} \approx 0.1 \text{ GeV}$  and  $\approx 0.22 \text{ GeV}$ , respec-

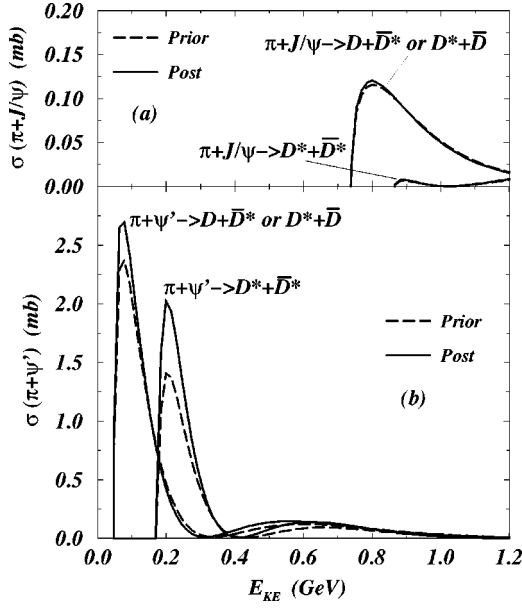


FIG. 5. Comparison of  $\pi+J/\psi$  and  $\pi+\psi'$  cross sections derived using post and prior formalisms.

tively [Fig. 6(b)]. It is interesting that the exclusive  $\psi'$  dissociation cross sections are very small near  $E_{KE}=0.3$  GeV (for the  $D\bar{D}^*$  final state) and 0.4 GeV (for the  $D^*\bar{D}^*$  final state), due to almost complete destructive interference between the diagrams and the nodes in the  $\psi'$  wave function.

The relative importance of the various terms in the Hamiltonian in these dissociation amplitudes is of course a very interesting question. Unfortunately it is also somewhat ambiguous, because the individual terms differ between post and prior formalisms; only the sum of all terms is formalism independent in nonrelativistic quantum mechanics. We find that the spin-spin interaction makes the dominant contribution to  $\pi+J/\psi$  dissociation in the prior formalism;  $\pi+\psi'$  dissociation in contrast is dominated by the linear confining interaction. In the post formalism we find that both  $\pi+J/\psi$  and  $\pi+\psi'$  are dominated by the spin-spin interaction. In all these cases the color-Coulomb contribution is subdominant.

Our results have interesting consequences for the survival of  $J/\psi$  and  $\psi'$  mesons propagating in a gas of pions. The pions produced in a heavy-ion collision have a roughly thermal distribution, with  $T\approx 200$  MeV in the nucleus-nucleus center-of-mass system, whereas heavy quarkonia such as the  $J/\psi$  and  $\psi'$  are produced approximately at rest. Thus the relative kinetic energy is typically a few hundred MeV. This is below the  $\pi+J/\psi$  dissociation threshold, but above that of  $\pi+\psi'$ , and in consequence we expect  $\pi+\psi'$  collisions to deplete the  $\psi'$  population much more effectively than  $\pi+J/\psi$  collisions reduce the initial  $J/\psi$  population. The weakness of  $\pi+J/\psi$  dissociation is further reduced by the small cross section we find for the  $\pi+J/\psi$  relative to  $\pi+\psi'$ .

Next we consider the very interesting exothermic collisions of charmonia with light vector mesons, specifically  $\rho+J/\psi$  and  $\rho+\psi'$ . Since the  $\rho$  meson has  $S=1$ , the total spin of the  $\rho+\{J/\psi \text{ or } \psi'\}$  system can be  $S_{tot}=\{0,1,2\}$ . This

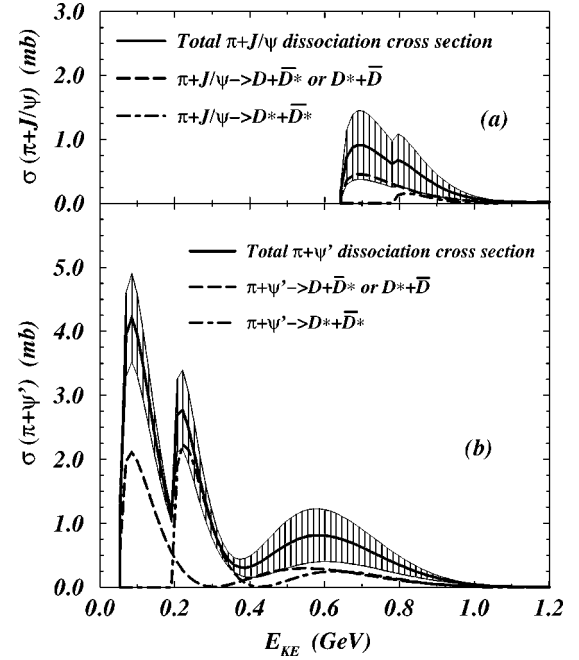


FIG. 6. Exclusive and total dissociation cross sections for  $\pi+J/\psi$  (a) and  $\pi+\psi'$  (b). In each panel the solid curve gives our estimated total cross section, which is the mean of the prior and post results.

$S_{tot}$  is conserved in our model and so must agree with the  $S_{tot}$  of the final state. The low-lying open charm final states are  $D\bar{D}$  with  $S_{tot}=0$ ,  $D\bar{D}^*$  and  $D^*\bar{D}$  with  $S_{tot}=1$ , and  $D^*\bar{D}^*$  with  $S_{tot}=\{0,1,2\}$ . The contribution of transitions to radially and orbitally excited final states will be considered in future work [43].

In the collision of an unpolarized  $\rho$  with an unpolarized  $J/\psi$ , the total dissociation cross section is comprised of contributions  $\sigma_f^{\text{unpol}}(S_{tot})$  from different final states  $f$  and different total spin values  $S_{tot}$ ,

$$\sigma_{tot}^{\text{unpol}} = \sum_f \sum_{S_{tot}} \sigma_f^{\text{unpol}}(S_{tot}), \quad (80)$$

where for this case with  $L_A=0$  and  $S_B=S_\rho\neq 0$  we can deduce from Eq. (17) the relationship

$$\sigma_f^{\text{unpol}}(S_{tot}) = \frac{(2S_{tot}+1)}{(2S_\rho+1)(2S_{J/\psi}+1)} \sigma_f(S_{tot}), \quad (81)$$

where  $\sigma_f(S_{tot})$  is the dissociation cross section for the final state  $f$  when the initial two-meson system is prepared with a total spin  $S_{tot}$ . [In our earlier work [21] for  $\rho+J/\psi$  and  $\rho+\psi'$  collisions,  $\sigma_f(S_{tot})$  results were presented and the total cross section of  $\sigma_{tot}=\sum_f \sum_{S_{tot}} \sigma_f(S_{tot})$  was evaluated. For collisions of unpolarized mesons one should use the unpolarized total dissociation cross section given by Eqs. (80) and (81).]

The unpolarized total  $\rho+J/\psi$  dissociation cross section is shown in Fig. 7(a). The exclusive cross sections  $\sigma_f^{\text{unpol}}(S_{tot})$  for dissociation into various final states are also shown. The

reaction  $\rho + J/\psi \rightarrow D\bar{D}$  is exothermic, so the cross section  $\sigma_{D\bar{D}}^{\text{unpol}}(S_{\text{tot}}=0)$  diverges as  $1/\sqrt{E_{KE}}$  as we approach threshold. For other  $\rho + J/\psi$  exclusive final states the thresholds lie at sufficiently higher energies to be endothermic. We find an unpolarized total  $\rho + J/\psi$  dissociation cross section of 2.4(0.4) mb at  $E_{KE}=0.1$  GeV, which has decreased to about 1.9 mb at  $E_{KE}=0.2$  GeV. At very low kinetic energies,  $J/\psi$  dissociation by  $\rho$  populates only the  $D\bar{D}(S_{\text{tot}}=0)$  final state. At slightly higher energies  $D\bar{D}^*$  and  $D^*\bar{D}(S_{\text{tot}}=1)$  final states dominate, and for  $E_{KE}$  above 0.2 GeV,  $D^*\bar{D}^*(S_{\text{tot}}=2)$  is dominant.

We have carried out similar calculations for  $\rho + \psi'$  collisions, and the results are shown in Fig. 7(b). In this case the reactions  $\rho + \psi' \rightarrow D\bar{D}, D\bar{D}^*, D^*\bar{D},$  and  $D^*\bar{D}^*$  are all exothermic, so all these exclusive cross sections  $\sigma_f^{\text{unpol}}(S_{\text{tot}})$  diverge as  $1/\sqrt{E_{KE}}$  as we approach threshold. The dominant dissociation channel is the  $D^*\bar{D}^*(S_{\text{tot}}=2)$  final state. The total unpolarized  $\rho + \psi'$  dissociation cross section falls from 4.5(0.1) mb at  $E_{KE}=0.1$  GeV to 1.5(0.3) mb at  $E_{KE}=0.2$  GeV and 0.4(0.2) mb at  $E_{KE}=0.3$  GeV.

In  $\rho + J/\psi$  dissociation the dominant scattering contribution in the prior formalism is due to the linear interaction. In the post formalism the dominant contribution arises from the color-Coulomb and linear interactions for energies  $E_{KE} < 0.1$  GeV, and from the color-Coulomb interaction for  $0.1 \text{ GeV} < E_{KE} < 0.4$  GeV, and from the spin-spin interaction for  $E_{KE} > 0.4$  GeV.

We next consider dissociation of  $J/\psi$  and  $\psi'$  through collisions with kaons. Our predictions for  $K + J/\psi$  and  $K + \psi'$  dissociation cross sections are shown in Fig. 8. The  $K + J/\psi$  process has a threshold kinetic energy of about 0.4 GeV, and the maximum cross section is about 0.7 mb. In  $K + \psi'$  dissociation the reactions are exothermic for the allowed final states  $D_s + \bar{D}^*, D_s^* + \bar{D},$  and  $D_s^* + \bar{D}^*$ . The total  $K + \psi'$  dissociation cross section, shown in Fig. 8(b), is about 1 mb at  $E_{KE} \sim 0.4$  GeV and diverges as  $1/\sqrt{E_{KE}}$  as we approach threshold.

## XI. CROSS SECTIONS FOR $Y$ AND $Y'$ DISSOCIATION.

It has been noted that a suppression of the production of  $b\bar{b}$  mesons such as the  $Y$  and  $Y'$  may also be useful as a signal for QGP production (see Ref. [32] and references cited therein). It is thus of interest to calculate  $Y$  and  $Y'$  dissociation cross sections in collisions with  $\pi, \rho,$  and  $K$  to estimate the importance of these comover dissociation processes.

In Fig. 9(a) we show the total cross section for  $\pi + Y$  dissociation. The threshold is at  $E_{KE} \sim 1$  GeV, and the maximum cross section is only about 0.05 mb. The small cross section arises from the combined effects of a large threshold and a small value of the strong interaction coupling constant. We show the dissociation cross section for  $\pi + Y'$  collisions in Fig. 9(b). It has a threshold of  $E_{KE} \sim 0.45$  GeV, and the peak cross section is about 5 mb near  $E_{KE} = 0.55$  GeV; this cross section is clearly much larger than  $\pi + Y$ .

In Fig. 10(a) we show the unpolarized cross section for  $\rho + Y$  dissociation. The unpolarized exclusive dissociation

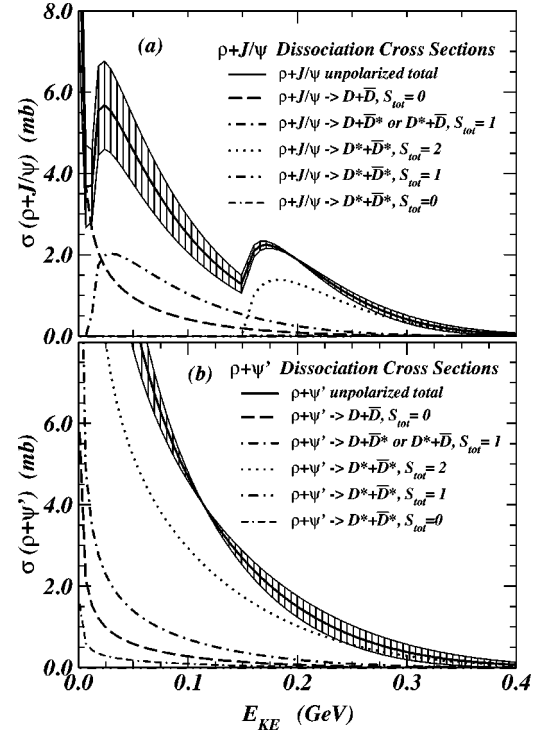


FIG. 7. The total unpolarized dissociation cross sections are shown as the solid curves for  $\rho + J/\psi$  in (a) and for  $\rho + \psi'$  in (b). Unpolarized exclusive dissociation cross sections  $\sigma_f^{\text{unpol}}(S_{\text{tot}})$  for different final states and different  $S_{\text{tot}}$  are also shown.

cross sections  $\sigma_f^{\text{unpol}}(S_{\text{tot}})$  for different final states and different  $S_{\text{tot}}$  are also shown. This reaction is endothermic, with a threshold at  $E_{KE} \sim 0.3$  GeV and a peak cross section of 0.15 mb at  $E_{KE} \sim 0.45$  GeV. In Fig. 10(b) we show the  $\rho + Y'$  dissociation cross section. The  $\rho + Y'$  reactions are exothermic, and the total dissociation cross section diverges as  $1/\sqrt{E_{KE}}$  near  $E_{KE} \sim 0$ , and is about 1.6 mb at  $E_{KE} \sim 0.2$  GeV.

In Fig. 11(a) we show the cross section for the  $K + Y$  dissociation. The threshold is at  $E_{KE} \sim 0.75$  GeV, with a peak total cross section of about 0.05 mb at  $E_{KE} \sim 0.85$  GeV.  $K + Y'$  is shown in Fig. 11(b); the threshold is at  $E_{KE} \sim 0.2$  GeV, with a peak total cross section of about 2 mb at  $E_{KE} \sim 0.25$  GeV.

## XII. CROSS SECTIONS FOR $\chi_J$ DISSOCIATION

We can similarly calculate the dissociation cross sections of the  $L=1$   $\chi_J c \bar{c}$  mesons with  $\pi, \rho,$  and  $K$  using the quark-interchange model. A  $\chi_J$  meson has spin  $S=1$  and a  $\pi$  has  $S=0$ , so a  $\pi + \chi_J$  collision yields a system with total spin  $S_{\text{tot}}=1$ . Since the interaction of Eq. (2) conserves total spin, the lowest-energy final states formed by  $\pi + \chi_J$  are  $D\bar{D}^*, D^*\bar{D},$  and  $D^*\bar{D}^*$ .

In Fig. 12 we show the dissociation cross sections for unpolarized  $\pi + \chi_J$  collisions. The unpolarized dissociation cross sections for the final states  $D\bar{D}^*$  and  $D^*\bar{D}^*$  are shown as dotted and dash-dotted curves, respectively. The unpolarized total cross sections for scattering into these lowest chan-

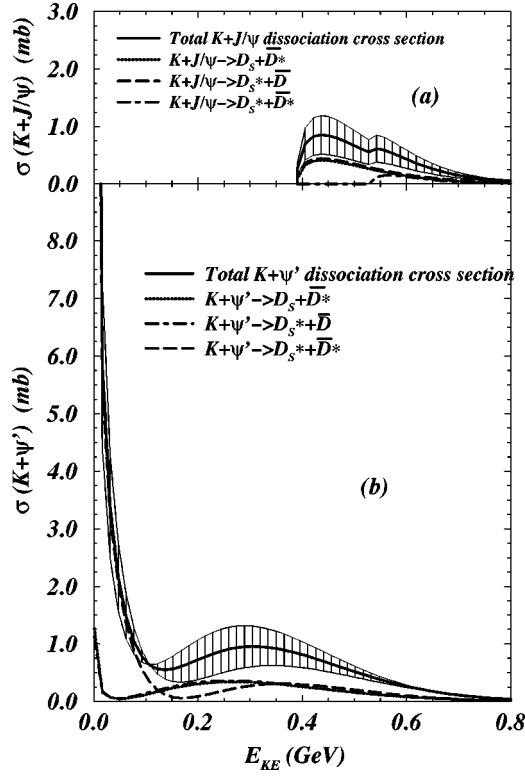


FIG. 8. Dissociation cross sections for  $K+J/\psi$  (a) and  $K+\psi'$  (b).

nels are shown as a solid curve. The dissociation process  $\pi+\chi_0$  has a threshold of  $E_{KE} \sim 0.32$  GeV and a peak cross section of 1.5 mb at  $E_{KE} \sim 0.5$  GeV [Fig. 12(a)];  $\pi+\chi_1$  has a threshold of  $E_{KE} \sim 0.23$  GeV and a peak dissociation cross section of 2.4 mb at  $E_{KE} \sim 0.46$  GeV [Fig. 12(b)],  $\pi+\chi_2$  and  $\pi+\chi_2$  has a threshold of  $E_{KE} \sim 0.18$  GeV and a peak dissociation cross section of about 3.0 mb at  $E_{KE} \sim 0.41$  GeV [Fig. 12(c)].

It is interesting to note that the maximum  $\pi+\chi_2$  unpolarized total dissociation cross section is only slightly greater than that of  $\pi+\chi_1$ , but is nearly twice as large as  $\pi+\chi_0$ . This indicates that the dissociation of  $\chi_J$  states is very sensitive to their masses. If the threshold for  $\pi+\chi_0$  were taken to be the same as for  $\pi+\chi_2$ , the unpolarized dissociation cross sections would be identical.

The dissociation amplitudes of the  $\chi_{JJ_z}$  mesons in collision with pions depend on  $J_z$ . A detailed discussion of the dissociation cross section for various  $J$  and  $J_z$  substates will be presented in [43]. The dependence on  $J_z$  is, however, quite weak. For given  $J$ , dissociation cross sections of  $\chi_{JJ_z}$  in collision with  $\pi$  vary only by a few percent for different  $J_z$ .

The thresholds for  $\pi+\chi_J$  dissociation lie between those of  $\pi+J/\psi$  and  $\pi+\psi'$ , and the maxima of the total dissociation cross sections for the  $\pi+\chi_J$  collisions are correspondingly greater than for  $\pi+J/\psi$  collisions but less than for  $\pi+\psi'$ .

In Fig. 13 we show unpolarized  $\rho+\chi_J$  dissociation cross sections. The lowest-lying final states are  $D\bar{D}$ ,  $D\bar{D}^*$ ,  $D^*\bar{D}$ , and  $D^*\bar{D}^*$ , characterized by different values of the total spin

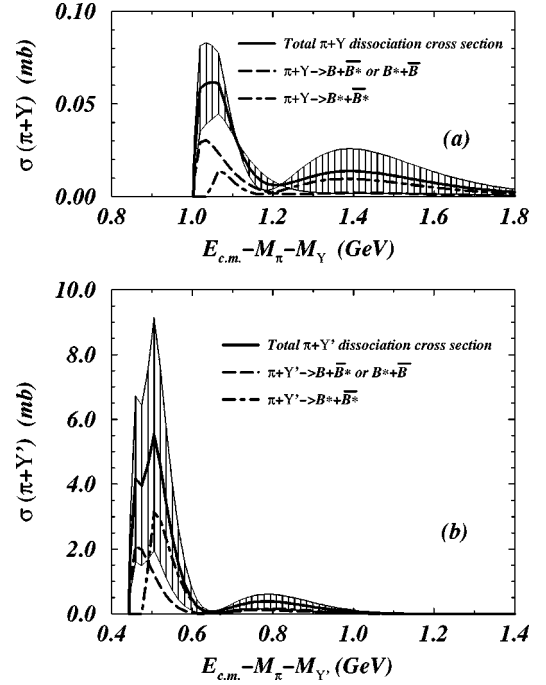


FIG. 9. The dissociation cross sections for  $Y$  (a) and  $Y'$  (b) in collision with  $\pi$ . Note that the scales of (a) and (b) are different.

$S_{tot}$ . The unpolarized total dissociation cross section is a sum of contributions  $\sigma_f^{\text{unpol}}(S_{tot})$  from different final states  $\{f\}$  and different total spins  $\{S_{tot}\}$ ,

$$\sigma_{tot}^{\text{unpol}} = \sum_f \sum_{S_{tot}} \sigma_f^{\text{unpol}}(S_{tot}), \quad (82)$$

where for this case, with  $L_A=1$  and  $S_B=1$ ,  $\sigma_f^{\text{unpol}}(S_{tot})$  is rather more complicated than the expression (81) for  $L_A=0$  and  $S_B=1$ . It can be determined from Eq. (15), and is given by

$$\sigma_f^{\text{unpol}}(S_{tot}) = \sum_{JM_A} (\hat{S}\hat{J})^2 \left\{ \begin{matrix} S_A & S_B & S \\ L_A & 0 & L_A \\ J_A & S_B & J \end{matrix} \right\}^2 \sigma(L_A M_A S S_z), \quad (83)$$

where  $\sigma(L_A M_A S S_z)$  is the cross section for an initial meson with total internal orbital angular momentum  $L_A$ , azimuthal component  $M_A$ , and total spin  $S$ . In Fig. 13 we show the unpolarized total dissociation cross section for  $\rho+\chi_0$ ,  $\rho+\chi_1$ , and  $\rho+\chi_2$ . Exclusive cross sections  $\sigma_f^{\text{unpol}}(S_{tot})$  for different final states and  $S_{tot}$  are also shown. Since  $\rho+\chi_J$  dissociation is exothermic, these cross sections have the common features that they diverge as  $1/\sqrt{E_{KE}}$  near  $E_{KE} \sim 0$  and decreases monotonically as  $E_{KE}$  increases. The dominant final state in these dissociation cross sections is  $D^*\bar{D}^*(S_{tot}=2)$ . The unpolarized total dissociation cross sections for  $\rho+\chi_0$  at  $E_{KE}=0.05, 0.1$ , and  $0.15$  GeV are 8.0 mb, 3.5 mb, and 1.6 mb, respectively [Fig. 13(a)]. For  $\rho+\chi_1$  at  $E_{KE}=0.05, 0.1$ , and  $0.15$  GeV these are 5.5 mb, 2.0 mb, and 0.8 mb, and for  $\rho+\chi_2$  at  $E_{KE}=0.05, 0.1$ , and  $0.15$  GeV are 4.3

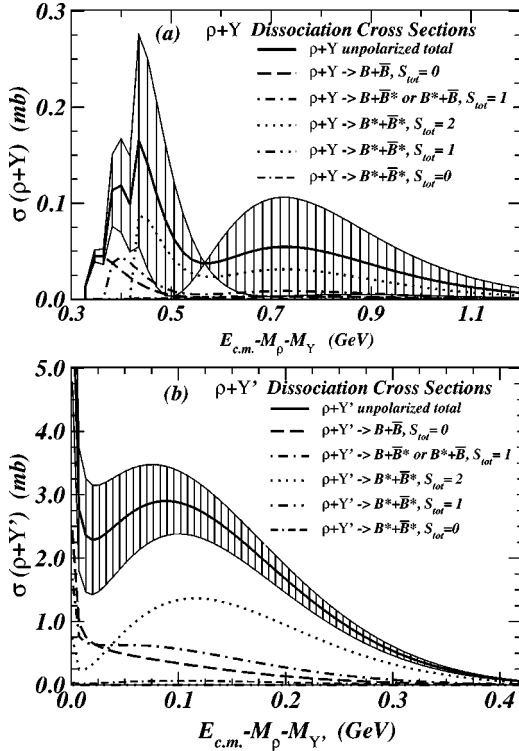


FIG. 10. Unpolarized total and exclusive dissociation cross sections  $\sigma_f^{\text{unpol}}(S_{tot})$  for  $\rho+Y$  (a) and  $\rho+Y'$  (b) for various channels and total spins  $S_{tot}$ . Note that (a) and (b) have different scales.

mb, 1.5 mb, and 0.5 mb. Thus, at a given kinetic energy  $E_{KE}$ ,  $\sigma_{tot}^{\text{unpol}}(\rho+\chi_0) > \sigma_{tot}^{\text{unpol}}(\rho+\chi_1) > \sigma_{tot}^{\text{unpol}}(\rho+\chi_2)$ .

In Fig. 14 we show the unpolarized dissociation cross sections for  $K+\chi_J$  collisions. The lowest-lying final states are  $D_s\bar{D}^*$ ,  $D_s^*\bar{D}$ , and  $D_s^*\bar{D}^*$ . For  $K+\chi_0$  dissociation the reaction has a threshold at 0.07 GeV. The total dissociation cross section rises from the threshold to a maximum cross section of 1.7 mb at 0.27 GeV [Fig. 14(a)]. In contrast,  $K+\chi_1$  and  $K+\chi_2$  collisions are exothermic to  $D_s\bar{D}^*$  and  $D_s^*\bar{D}$ . Thus these also behave as  $1/\sqrt{E_{KE}}$  near  $E_{KE} \sim 0$ , but decrease rapidly as  $E_{KE}$  increases. These cross sections then vary slowly up to  $E_{KE} \sim 0.2$  GeV before decreasing at higher kinetic energies.

### XIII. DISCUSSION AND CONCLUSIONS

We have used the Barnes-Swanson quark-interchange model, with parameters taken from fits to meson spectroscopy, to evaluate the low-energy cross sections for the dissociation of  $J/\psi$ ,  $\psi'$ ,  $\chi$ ,  $Y$ , and  $Y'$  in collision with  $\pi$ ,  $\rho$ , and  $K$ . The cross sections obtained here should be useful as estimates of the importance of “comover” scattering in suppressing heavy-quarkonium production, which is of considerable interest in the search for the quark-gluon plasma.

The threshold for the dissociation of  $J/\psi$  by  $\pi$  is relatively high, and the peak total cross section is about 1 mb. In contrast, dissociation of  $\psi'$  by  $\pi$  opens at a low threshold and the cross section is much larger. We have also evaluated the corresponding cross sections for the dissociation by  $\rho$ .

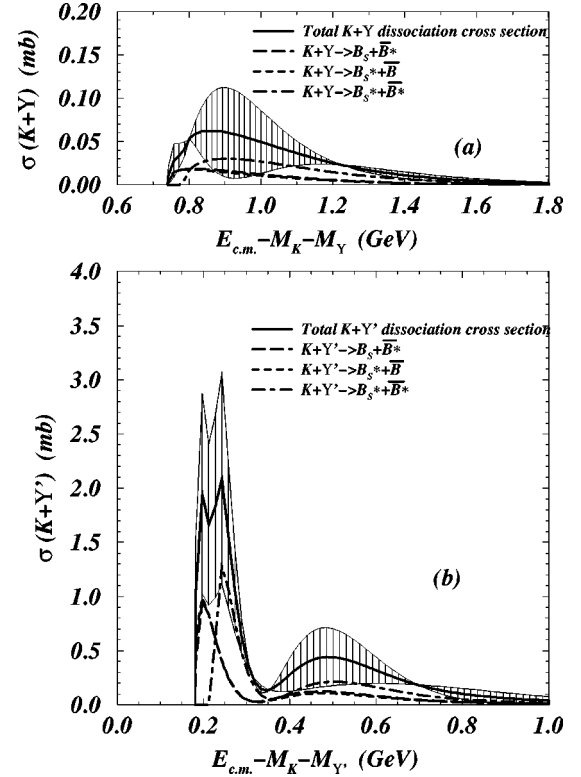


FIG. 11. The dissociation cross sections for  $K+Y'$  (a) and  $K+Y$  (b) to various final states. Note that (a) and (b) have different scales.

These processes are exothermic and have large total dissociation cross sections that diverge at threshold.

We previously noted that our  $\pi+J/\psi$  cross section is considerably smaller than the estimate of Ref. [20], although we use a similar approach. There are several differences between the two approaches that lead to this discrepancy. First, Martins *et al.* assumed that the confining interaction is an attractive Gaussian potential which acts only between quark-antiquark pairs. The neglect of the quark-quark and antiquark-antiquark confining interactions discards the transfer diagrams (T1 and T2) for the confining potential. Since we find that the transfer and capture diagram confinement contributions are similar in magnitude but opposite in sign (due to color matrix elements), the confining interaction assumed by Martins *et al.* did not incorporate an important destructive interference. Second, their use of a Gaussian, rather than the usual linear confining potential, obviously leads to quantitatively different cross sections.

The destructive interference between transfer and capture diagrams with spin-independent forces (color-Coulomb and confinement) has been noted previously. See, for example, Refs. [33,34] and references cited in [37]. This interference explains the well-known spin-spin hyperfine dominance in light-hadron scattering in channels such as  $I=2 \pi\pi$  and the core  $NN$  interaction. With heavy quarks, however, the hyperfine interaction contribution is smaller due to the large charm quark mass; for this reason we included the color-Coulomb and confining interactions in our analysis. Our results indicate that the spin-spin, linear confining, and color-Coulomb

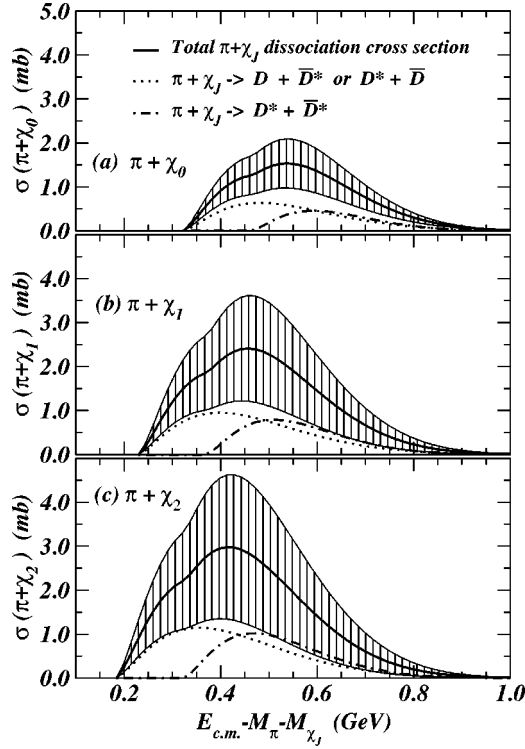


FIG. 12. Unpolarized total cross sections and exclusive unpolarized cross sections for the dissociation reactions  $\pi + \chi_J$  into  $D + \bar{D}^*$  and  $D^* + \bar{D}^*$ . (a)  $\pi + \chi_0$ , (b)  $\pi + \chi_1$ , and (c)  $\pi + \chi_2$ .

interactions all give important contributions to the dissociation cross sections.

It is of interest to compare our results for dissociation cross sections to those obtained for meson-exchange models with effective Lagrangians [24–27]. In the effective Lagrangian approach, the dissociation cross section increases with energy, as expected for the  $t$ -channel exchange of a pointlike spin-1 particle. For example in Ref. [26] the dissociation cross section is about 30 mb for  $\pi + J/\psi \rightarrow D + \bar{D}^*$  and about 80 mb for  $\pi + Y \rightarrow B + \bar{B}^*$  at 1 GeV above the threshold. These large cross sections continue to increase with increasing energy. In contrast, in our quark model calculation using the Barnes-Swanson model, we find very small cross sections this far above threshold for  $\pi + J/\psi \rightarrow D + \bar{D}^*$  and  $\pi + Y \rightarrow B + \bar{B}^*$ . The predicted peak cross section for  $\pi + J/\psi \rightarrow D + \bar{D}^*$  is about 0.5 mb and occurs at about 0.05 GeV above the threshold. The predicted peak cross section for  $\pi + Y \rightarrow B + \bar{B}^*$  is even smaller (about 0.03 mb), and it occurs at about 0.02 GeV above the threshold. These cross sections decrease rapidly at higher energies. Thus, the large cross sections obtained in the effective Lagrangian approach differ by orders of magnitude from our quark model results. We believe that the large and increasing dissociation cross sections predicted by the effective Lagrangian meson exchange models at high energies is unrealistic, since the momentum distributions of the boosted final and the initial meson states will in practice have little overlap at high energies. One should not relate physical cross section to effective Lagrangian model without form factors. As

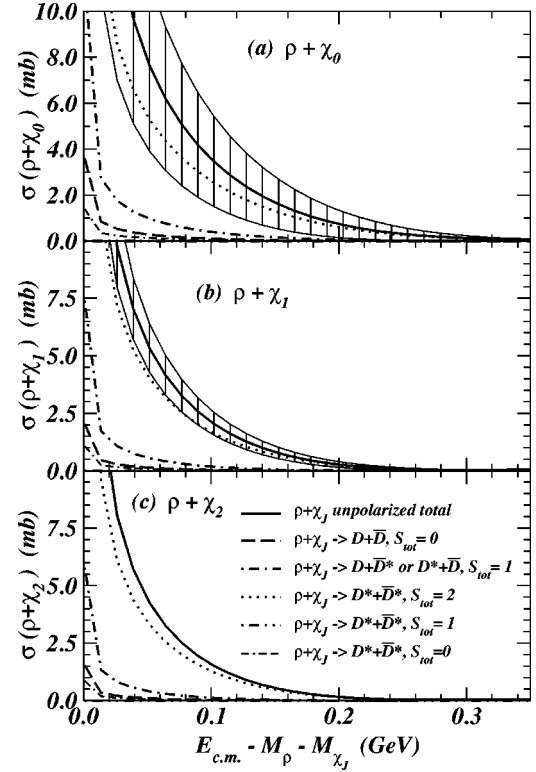


FIG. 13. Unpolarized total cross sections and unpolarized exclusive cross sections  $\sigma_f^{\text{unpol}}(S_{tot})$  for the dissociation reactions  $\rho + \chi_J$  into  $D\bar{D}$ ,  $D + \bar{D}^*$ , and  $D^* + \bar{D}^*$ . (a)  $\rho + \chi_0$ , (b)  $\rho + \chi_1$ , and (c)  $\rho + \chi_2$ .

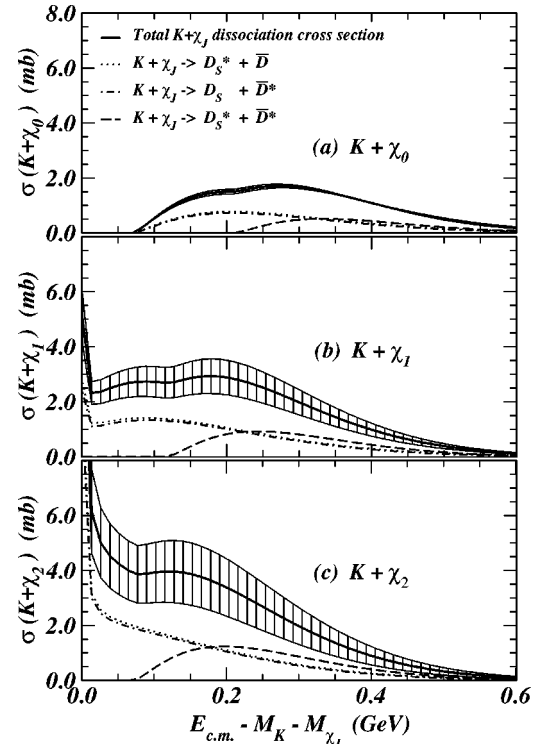


FIG. 14. Unpolarized cross sections for the dissociation reactions  $K + \chi_J$ . (a)  $K + \chi_0$ , (b)  $K + \chi_1$ , and (c)  $K + \chi_2$ .

TABLE IV. Coefficients  $\{a_n\}$  for each meson in an  $N=6$  basis.

Meson	$M$ (expt) (GeV)	$M$ (th) (GeV)	$\sqrt{\langle r^2 \rangle}$ (fm)	$\beta$ (GeV)	$a_1$	$a_2$	$a_3$	$a_4$	$a_5$	$a_6$
$\pi$	0.140	0.140	0.512	0.380	0.8288	-0.5178	-0.2294	4.0001	-5.8837	2.9139
$K$	0.494	0.495	0.521	0.440	1.4258	-2.9104	6.6580	-7.6222	4.1972	-0.6622
$K^*$	0.892	0.904	0.674	0.440	2.6690	-7.7381	18.5854	-25.2611	17.6588	-4.9261
$\rho$	0.770	0.774	0.769	0.380	2.5214	-6.9921	16.7985	-22.9186	16.1163	-4.5409
$\phi(1s)$	1.020	0.992	0.647	0.380	1.4078	-2.2292	5.2488	-6.4976	4.0718	-0.9727
$b_1$	1.235	1.330	0.978	0.380	2.2568	-5.4759	12.6496	-17.1515	12.1528	-3.4443
$a_1$	1.260	1.353	0.993	0.380	2.3362	-5.7733	13.3524	-18.2221	13.0172	-3.7466
$\phi(2s)$	1.686	1.870	0.983	0.380	5.7964	-24.6635	58.1365	-79.9357	56.8725	-16.2428
$D$	1.869	1.913	0.585	0.440	1.8275	-4.2160	10.0225	-13.0384	8.6764	-2.2285
$D^*$	2.010	1.998	0.626	0.440	2.1630	-5.4765	13.0711	-17.5068	12.0520	-3.2893
$D_s$	1.969	2.000	0.508	0.440	1.0701	-1.1418	2.4522	-1.9688	0.3196	0.3292
$D_s^*$	2.112	2.072	0.546	0.440	1.3267	-1.9616	4.5086	-5.2172	2.9478	-0.5646
$D_1(^1P_1)$	2.422	2.506	0.840	0.440	2.2042	-5.2226	12.0872	-16.4595	11.7325	-3.3595
$D_2(^3P_2)$	2.460	2.514	0.845	0.440	2.2344	-5.3296	12.3210	-16.7896	11.9756	-3.4375
$\eta_c$	2.979	3.033	0.388	0.560	0.9461	-0.6474	1.0666	0.3614	-1.6509	0.9868
$J/\psi$	3.097	3.069	0.404	0.560	1.0786	-1.0517	2.0729	-1.2289	-0.3804	0.5646
$h_c$	3.570	3.462	0.602	0.560	1.6312	-2.8587	6.7068	-9.0601	6.4161	-1.8163
$\chi_c$	3.525	3.466	0.606	0.560	1.6587	-2.9420	6.8805	-9.3051	6.5918	-1.8698
$\psi'$	3.686	3.693	0.666	0.560	5.5237	-22.5889	53.5145	-74.6754	53.9666	-15.7222
$B$	5.279	5.322	0.574	0.500	2.4905	-7.0584	17.0138	-23.0809	16.1128	-4.4690
$B^*$	5.324	5.342	0.583	0.500	2.5806	-7.4190	17.8694	-24.2889	16.9859	-4.7275
$B_s$	5.369	5.379	0.503	0.500	1.6289	-3.2614	7.6922	-9.8055	6.3702	-1.5866
$B_s^*$	5.416	5.396	0.513	0.500	1.7111	-3.5483	8.3718	-10.7991	7.1136	-1.8177
$Y(1s)$	9.460	9.495	0.255	0.660	0.1364	2.0441	-6.7818	14.2875	-13.9803	5.3693
$\chi_b(1p)$	9.899	9.830	0.423	0.660	0.7416	0.1481	0.2178	-0.0196	-0.1923	0.1587
$Y(2s)$	10.020	9.944	0.519	0.660	-3.6422	10.7655	-25.3407	38.7395	-30.5647	9.8544
$\chi_b(2p)$	10.260	10.166	0.604	0.660	3.2645	-10.1170	20.7960	-28.2373	20.2666	-5.9472

the effective Lagrangian approach does not contain information about the internal structure of the interacting hadrons, form factors have been introduced phenomenological to reduce the theoretical cross sections [25–27]. A realistic description of the form factors should incorporate the meson wave functions and the dynamics of the scattering process. Without a derivation of these form factors, one encounters considerable uncertainty, as experimental data on these reaction processes are unavailable. The form factors introduced in [25–27] lead to changes of the theoretical cross section at high energies by several orders of magnitude. The results are sensitive to the assumed coupling strength and to the functional dependence assumed for the form factor. In view of the strong dependence of the theoretical results on the form factor and the coupling constants, a careful determination of these quantities are required in future work.

Although there are no direct experimental measurements of these low-energy cross sections to which we can compare our results, the small  $\pi+J/\psi$  and large  $\pi+\psi'$  dissociation cross sections obtained here at low kinetic energies appear qualitatively consistent with earlier results found in a microscopic model of  $J/\psi$  and  $\psi'$  suppression in O+A and S+U collisions [8,9]. Hopefully, future Monte Carlo simulations of the dynamics of charmonium in heavy-ion collisions will lead to more direct comparisons. It is interesting to note

that dissociation of the  $J/\psi$  by  $\pi$  and  $\rho$  populate different states (for example,  $\pi+J/\psi$  does not lead to  $D\bar{D}$  in our model but  $\rho+J/\psi$  does). It may be possible to separate these processes by studying the relative production of  $D\bar{D}$ ,  $D^*\bar{D}$ ,  $D\bar{D}^*$ , and  $D^*\bar{D}^*$ , if the open charm background can be subtracted. The large ratio of initial open charm to  $J/\psi$  production in a nucleon-nucleon collision may however make this separation very difficult.

It may be useful in the future to carry out detailed simulations of  $J/\psi$  absorption in heavy-ion collisions using the cross sections obtained here. If our cross sections do prove to be reasonably accurate, it will be useful to incorporate them in simulations of hadronic processes in relativistic heavy-ion collisions to isolate  $J/\psi$  suppression due to interactions with hadronic matter.

It should be noted that in addition to the quark-interchange processes considered in this paper, low-energy meson-meson scattering more generally will involve  $s$ -channel processes with intermediate resonances, such as  $\pi+\pi\rightarrow\rho\rightarrow\pi+\pi$ . The  $s$ -channel process can be treated by introducing a pair production and annihilation amplitude, as was previously considered by Ackleh, Barnes, and Swanson [44]. It will be of interest in the future to extend the present quark-based model to reactions involving pair annihilation

and production. Such an extension will allow us to evaluate many additional cross sections of interest in high-energy heavy-ion collisions.

### ACKNOWLEDGMENTS

This research was supported by the Division of Nuclear Physics, Department of Energy, under Contract No. DE-AC05-00OR22725 managed by UT-Battelle, LLC. E.S. acknowledges support from the DOE under Grant No. DE-FG02-00ER41135 and DOE Contract No. DE-AC05-84ER40150 under which the Southeastern Universities

Research Association operates the Thomas Jefferson National Accelerator Facility. The authors would also like to thank Dr. C. M. Ko, Dr. H. Crater, and Dr. S. Sorensen for useful discussions.

### APPENDIX: TABULATION OF BOUND-STATE WAVE FUNCTIONS

The coefficients  $\{a_n\}$  for each meson in an  $N=6$  basis, with a different  $\beta$  for each meson, are listed in Table IV.

- 
- [1] *Quark Matter '99*, Proceedings of the 14th International Conference on Ultra-Relativistic Nucleus-Nucleus Collisions, edited by L. Riccati, M. Maserà, and E. Vercellin [Nucl. Phys. **A661**, 1 (1999)].
- [2] C. Y. Wong, *Introduction to High-Energy Heavy-Ion Collisions* (World Scientific, Singapore, 1994).
- [3] U. Heinz and M. Jacobs, nucl-th/0002042.
- [4] C.Y. Wong, Nucl. Phys. **A681**, 22c (2001).
- [5] T. Matsui and H. Satz, Phys. Lett. B **178**, 416 (1986).
- [6] M. Gonin, NA50 Collaboration, Nucl. Phys. **A610**, 404c (1996).
- [7] A. Romana *et al.*, NA50 Collaboration, Proceedings of the XXXIII Recontres de Moriond, Les Arcs, France, 1998.
- [8] C.Y. Wong, Nucl. Phys. **A610**, 434c (1996); **A630**, 487 (1998).
- [9] C.Y. Wong, Proceedings of Workshop on Charmonium Production in Relativistic Nuclear Collisions, INT, Seattle, 1998, hep-ph/9809497.
- [10] D. Kharzeev, Nucl. Phys. **A610**, 418c (1996); **A638**, 279c (1998).
- [11] J.-P. Blaizot and J.-Y. Ollitrault, Nucl. Phys. **A610**, 452c (1996).
- [12] A. Capella, A. Kaidalov, A.K. Akil, and C. Gerschel, Phys. Lett. B **393**, 431 (1997).
- [13] W. Cassing and C.M. Ko, Phys. Lett. B **396**, 39 (1997); W. Cassing and E.L. Bratkovskaya, Nucl. Phys. **A623**, 570 (1997).
- [14] R. Vogt, Phys. Lett. B **430**, 15 (1998).
- [15] M. Nardi and H. Satz, Phys. Lett. B **442**, 14 (1998).
- [16] Bin Zhang, C.M. Ko, Bao-An Li, Ziwei Lin, and Ben-Hao Sa, Phys. Rev. C **62**, 054905 (2000).
- [17] D.B. Blaschke, G.R.G. Burau, M.I. Ivanov, Yu.L. Kalinovsky, and P.C. Tandy, Phys. Lett. B **506**, 297 (2001).
- [18] D. Kharzeev and H. Satz, Phys. Lett. B **334**, 155 (1994).
- [19] D. Kharzeev, H. Satz, A. Syamtomov, and G. Zinovjev, Phys. Lett. B **389**, 595 (1996).
- [20] K. Martins, D. Blaschke, and E. Quack, Phys. Rev. C **51**, 2723 (1995).
- [21] C.Y. Wong, E.S. Swanson, and T. Barnes, Phys. Rev. C **62**, 045201 (2000).
- [22] C.Y. Wong, E.S. Swanson, and T. Barnes, Proceedings of the Hirscheegg 2000 Workshop on Hadrons in Dense Matter, Hirscheegg, Austria, 2000, nucl-th/000203.
- [23] T. Barnes, E.S. Swanson, and C.Y. Wong, Proceedings of the International Workshop on Heavy Quark Physics 5, Dubna, 2000, nucl-th/0006012.
- [24] S.G. Matinyan and B. Müller, Phys. Rev. C **58**, 2994 (1998).
- [25] K.L. Haglin, Phys. Rev. C **61**, 031912(R) (2000); K.L. Haglin and C. Gale, *ibid.* **63**, 065201 (2001).
- [26] Z.W. Lin and C.M. Ko, Phys. Rev. C **62**, 034903 (2000).
- [27] Yongseok Oh, Taesoo Song, and Su Hong Lee, Phys. Rev. C **63**, 034901 (2001).
- [28] A. Sibirtsev, K. Tsushima, and A.W. Thomas, Phys. Rev. C **63**, 044906 (2001).
- [29] M. Peskin, Nucl. Phys. **B156**, 365 (1979).
- [30] G. Bhanot and M. Peskin, Nucl. Phys. **B156**, 391 (1979).
- [31] L. Antoniazzi *et al.*, Phys. Rev. Lett. **70**, 383 (1993).
- [32] Ziwei Lin and C.M. Ko, Phys. Lett. B **503**, 104 (2001).
- [33] T. Barnes and E.S. Swanson, Phys. Rev. D **46**, 131 (1992).
- [34] E.S. Swanson, Ann. Phys. (N.Y.) **220**, 73 (1992).
- [35] T. Barnes, E.S. Swanson, and J. Weinstein, Phys. Rev. D **46**, 4868 (1992).
- [36] T. Barnes and E.S. Swanson, Phys. Rev. C **49**, 1166 (1994).
- [37] T. Barnes, S. Capstick, M.D. Kovarik, and E.S. Swanson, Phys. Rev. C **48**, 539 (1993).
- [38] T. Barnes, N. Black, D.J. Dean, and E.S. Swanson, Phys. Rev. C **60**, 045202 (1999).
- [39] L. I. Schiff, *Quantum Mechanics* (McGraw-Hill, New York, 1968), pp. 384–387.
- [40] A. de-Shalit and I. Talmi, *Nuclear Shell Model* (Academic, New York, 1963).
- [41] W. Hoogland *et al.*, Nucl. Phys. **B126**, 109 (1977).
- [42] C.Y. Wong and H. Crater, Phys. Rev. C **63**, 044907 (2001).
- [43] T. Barnes, E. S. Swanson, and C. Y. Wong (unpublished).
- [44] E.S. Ackleh, T. Barnes, and E. S. Swanson, Phys. Rev. D **54**, 6811 (1996).